

**OPTIMAL OPERATION STRATEGIES OF
TRANSFORMERS FOR THIRD RAIL SYSTEM TO
IMPROVE ENERGY EFFICIENCY**

TAN ZHI HAO

MASTER OF ENGINEERING SCIENCE

**LEE KONG CHIAN FACULTY OF ENGINEERING AND
SCIENCE
UNIVERSITI TUNKU ABDUL RAHMAN
AUGUST 2021**

**OPTIMAL OPERATION STRATEGIES OF TRANSFORMERS FOR
THIRD RAIL SYSTEM TO IMPROVE ENERGY EFFICIENCY**

By

TAN ZHI HAO

A dissertation submitted to the Department of Electrical and Electronic
Engineering,
Lee Kong Chian Faculty of Engineering and Science,
Universiti Tunku Abdul Rahman,
In partial fulfillment of the requirements for the degree of Master of
Engineering Science
August 2021

ABSTRACT

OPTIMAL OPERATION STRATEGIES OF TRANSFORMERS FOR THIRD RAIL SYSTEM TO IMPROVE ENERGY EFFICIENCY

Tan Zhi Hao

The energy efficiency of railway systems is essentially important in lowering down the operational costs as well as reducing the carbon emission towards sustainable development. A typical third rail DC railway system is supplied from bulk supply substations (BSS) that are connected to the main grid. Thus, to maintain the reliability of the railway traction power systems, the BSSs are usually designed with additional power transformers in main-tie-main configuration. There are three operational modes for these transformers, namely non-parallel mode, parallel mode, and single transformer mode. Due to the fact that the traction loads are inherently dynamic, the optimal operation mode for the transformers requires a thorough simulation by including the train dynamics and train schedules. In this study, a comprehensive electrical model that includes the low voltage traction network and high voltage supply network of the Mass Rapid Transit 2 (MRT2) in Malaysia is developed. The model is developed using ETAP-Etrax software for dynamic load flow simulations to achieve an accurate estimation of transformer losses under the three transformer operation modes. The effects of train schedules to operating efficiency of transformer modes are investigated by including train headway interval variations. The results showed that the parallel mode has lower transformer losses than that of non-parallel

mode for all the headway intervals, with a maximum loss reduction of up to 6.52%. It is also found that the single transformer mode has the lowest transformer losses for headway intervals of 5 minutes 48 seconds and above. Although the percentage of transformer loss reduction and the headway interval margin for optimal operation of single transformer mode may differ, this approach can also be applied to other DC railway systems.

ACKNOWLEDGEMENTS

First and foremost, I would like to express my gratitude to my supervisor, Dr. Chua Kein Huat, for his professional guidance throughout this research work. He does not hesitate to share with his experiences in academic research, particularly on how to tackle problems and to identify research gaps. This thesis would take a much longer time to be completed without his generous and professional assistance. His teachings are not only limited to this research work. He helps me in developing the individual moral values and proper behaviours by being the role model. He also tries his best to strive for the opportunities for me to participate in events which he deemed constructive to me. I would also like to thank my co-supervisor, Prof. Ir. Dr. Lim Yun Seng, for his patient guidance and constructive suggestions, particularly in my paper writings. I would like to express my gratitude to Colas Rails System Engineering Sdn. Bhd. for awarding me fund for this research work, and their willingness to disclose all the required technical data to me. I am particularly grateful to my parents, siblings, and relatives for their love and support. I would also like to show my special thanks to my postgraduate seniors Soon Kok Yew, Yvonne Oon Li Voon, and Daniel Toh Chia Ming, who have helped me a lot during my master degree's study. Finally, I would also like to thank the faculty and staffs for their support throughout my graduate career.

APPROVAL SHEET

This dissertation entitled “OPTIMAL OPERATION STRATEGIES OF TRANSFORMERS FOR THIRD RAIL SYSTEM TO IMPROVE ENERGY EFFICIENCY” was prepared by TAN ZHI HAO and submitted as partial fulfillment of the requirements for the degree of Master of Engineering Science at Universiti Tunku Abdul Rahman.

Approved by:



(Dr. CHUA KEIN HUAT)

Supervisor

Department of Electrical and Electronic Engineering
Lee Kong Chian Faculty of Engineering and Science
Universiti Tunku Abdul Rahman

Date: 22/8/2021



(Prof. Ir. Dr. LIM YUN SENG)

Co-supervisor

Department of Electrical and Electronic Engineering
Lee Kong Chian Faculty of Engineering and Science
Universiti Tunku Abdul Rahman

Date: 24/8/2021

LEE KONG CHIAN FACULTY OF ENGINEERING AND SCIENCE
UNIVERSITI TUNKU ABDUL RAHMAN

Date: 22/8/2021

SUBMISSION SHEET
SUBMISSION OF DISSERTATION

It is hereby certified that **TAN ZHI HAO** (ID No: 19UEM04760) has completed this dissertation entitled “OPTIMAL OPERATION STRATEGIES OF TRANSFORMERS FOR THIRD RAIL SYSTEM TO IMPROVE ENERGY EFFICIENCY” under the supervision of Dr. Chua Kein Huat (Supervisor) from the Department of Electrical and Electronic Engineering, Lee Kong Chian Faculty of Engineering and Science, and Prof. Ir. Dr. Lim Yun Seng (Co-supervisor) from the Department of Electrical and Electronic Engineering, Lee Kong Chian Faculty of Engineering and Science.

I understand that University will upload softcopy of my dissertation in PDF format into UTAR Institutional Repository, which may be made accessible to UTAR community and the public.

Yours truly,



(*Tan Zhi Hao*)

DECLARATION

I (TAN ZHI HAO) hereby declare that the dissertation is based on my original work except for quotations and citations which have been duly acknowledged. I also declare that it has not been previously or concurrently submitted for any other degree at UTAR or other institutions.



(TAN ZHI HAO)

Date: 22/8/2021

TABLE OF CONTENTS

	Page
ABSTRACT	iii
ACKNOWLEDGEMENTS	v
APPROVAL SHEET	vi
SUBMISSION SHEET	vii
TABLE OF CONTENTS	ix
LIST OF TABLES	xi
LIST OF FIGURES	xiii
LIST OF ABBREVIATIONS	xvi
CHAPTER 1 INTRODUCTION	1
1.1 Research Background	1
1.2 Research objectives	6
1.3 Scope of research	7
1.4 Dissertation organisation	7
1.5 List of Publications	9
CHAPTER 2 LITERATURE REVIEW	11
2.1 DC Traction Power Systems	11
2.2 Energy Saving on Railway Systems	12
2.2.1 Regenerative Braking	12
2.2.2 Energy Efficient Driving	20
2.2.3 Loss Reduction on Supply Network	23
2.3 Parallel Transformer Operation	24
CHAPTER 3 METHODOLOGY	29
3.1 Introduction	29
3.2 Modelling of the High Voltage Railway Traction Power System	32
3.2.1 Bulk Supply Substations (BSS)	32
3.2.2 Traction Power Substations (TPSS)	37
3.2.3 Utility Buildings	43
3.3 BSS Transformers Operation Modes	44
3.4 Transformer Efficiency Calculations	49
3.5 Dynamic Traction Load Modelling	52
3.6 Short-circuit Analyses	73
CHAPTER 4 RESULTS AND DISCUSSIONS	77
4.1 Introduction	77

4.2 Train Dynamic Profiles	77
4.3 BSS Transformer Loadings and Losses	81
4.4 Impacts of Headway Variation	85
4.5 Short-circuit Analyses	90
4.6 Investment Cost for Parallel Mode	98
CHAPTER 5 CONCLUSION AND FUTURE WORKS	99
5.1 Conclusion	99
5.2 Limitations and future works	103
LIST OF REFERENCES	105

LIST OF TABLES

Table		Page
1.1	List of publications	10
3.1	Number of TPSS and utility building connected to each BSS.	32
3.2	Key parameters of BSS transformers	34
3.3	Key parameters of earthing transformers	36
3.4	Key parameters of BSS cables	37
3.5	Key parameters of rectifier transformers	38
3.6	Key parameters of medium voltage network cables	40
3.7	Key parameters for AC-DC converters	40
3.8	Key parameters of auxiliary transformers	43
3.9	Losses on 132/33 kV BSS transformers	51
3.10	Parameters of the rolling stock for MRT2	56
3.11	Davis coefficient of MRT2 train used in ETAP software	61
3.12	Voltage factor 'c' as per IEC 60909	74
3.13	Short-circuit current contribution X/R ratio by the grid	76
3.14	Rated short-time withstand current for different switchgear	76
4.1	Train arrival and departure time for northbound	80
4.2	Train arrival and departure time for southbound	81
4.3	Peak and average loading of the BSS transformers in parallel and non-parallel modes	83
4.4	Peak and average loading of the BSS transformers in single transformer mode	84

4.5	1-hour transformer losses for all three operation modes	84
4.6	Total transformer losses at different headway for non-parallel mode and parallel mode	87
4.7	Total transformer losses at different headway for non-parallel mode and single transformer mode	88
4.8	Total transformer losses at different headway for parallel mode and single transformer mode	89
4.9	Short-circuit current for fault at 132 kV level for non-parallel mode	99
4.10	Short-circuit current for fault at 132 kV level for parallel mode	92
4.11	Short-circuit current for fault at BSSs at 33 kV level	93

LIST OF FIGURES

Figures		Page
1.1	Passenger rail transport activity by fuel type from the year 1995-2016	2
2.1	Utilisation of regenerative energy from the power-time profile of two trains	15
2.2	Relationship between train travel time and minimum energy consumption	21
2.3	PLO point of two transformers with different power ratings	27
3.1	The map of the MRT2 route	29
3.2	(a) schematic view (b) geospatial view	31
3.3	Schematic diagram of a BSS with transformers	33
3.4	2-winding Transformer Editor in ETAP	35
3.5	Schematic diagram of a TPSS	37
3.6	3-winding Transformer Editor in ETAP	39
3.7	AC-DC Converter Editor in ETAP	41
3.8	Lumped Load Editor in ETAP	42
3.9	Schematic diagram of a utility building	44
3.10	Configuration for non-parallel mode	45
3.11	Configuration for parallel mode	46
3.12	Configuration for single transformer mode	46
3.13	Configuration for emergency scenario (Jinjang BSS outage)	47
3.14	Configuration for emergency scenario (Kuchai Lama BSS outage)	48
3.15	Configuration for emergency scenario (UPM BSS outage)	48

3.16	User interface of Configuration Manager in ETAP	49
3.17	Efficiency curve for transformer rated 50 MVA at a power factor of 0.95	52
3.18	The Jinjang BSS section on the Map	53
3.19	Structure of tracks of the third rail system	54
3.20	Schematic diagram of the low voltage traction network	55
3.21	Train Rolling Stock Library in ETAP	57
3.22	Tractive effort curve in Train Rolling Stock Library	58
3.23	Tractive effort curve	63
3.24	Braking effort curve	64
3.25	Track models in Geospatial Diagram	66
3.26	Elevation Marker Editor in ETAP	67
3.27	Stations and track elevations	67
3.28	Speed Limit Marker Editor in ETAP	68
3.29	Speed limit along the line for (a) northbound (b) southbound	69
3.30	Configure train timetables in Etrax Editor	71
3.31	Load flow calculation with train dynamics	72
3.32	Short-circuit Study Case Editor in ETAP	75
4.1	Single train speed profile for (a) northbound (b) southbound	78
4.2	Single train power profile for (a) northbound (b) southbound	79
4.3	BSS transformer demand profile for non-parallel mode and parallel mode	82
4.4	System total energy consumption at different headways	86

4.5	Transformer losses for different operation modes at different headway intervals	90
4.6	Short-circuit current for fault at all TPSSs	94
4.7	Short-circuit current of Jinjang BSS outage and normal scenario parallel mode	96
4.8	Short-circuit current of Kuchai Lama BSS outage and normal scenario parallel mode	96
4.9	Short-circuit current of UPM BSS outage and normal scenario parallel mode	97

LIST OF ABBREVIATIONS

ACO	Ant Colony Optimisation
ALSS	Aluminium/stainless steel
ANN	Artificial neural network
ATO	Automatic train operation
BSS	Bulk supply substation
CO ₂	Carbon dioxide
DP	Dynamic programming
eSCADA	Electrical Supervisory Control and Data Acquisition
ESS	Energy storage system
GA	Genetic algorithm
HTSC	High-temperature superconducting
IABC	Improved Artificial Bee Colony
IPT	Interphase transformer
LGM	Lagrange multipliers
MRT2	Mass Rapid Transit 2
OBESS	On-board energy storage system
PLO	Parallel losses optimisation
PSO	Particle Swarm Optimisation
RTCC	Remote Tap Changer Control Cucible
SESS	Stationary energy storage system
SiC	Silicon carbide
SOC	State-of-charge
TPSS	Traction power substations

WESS Wayside energy storage system

CHAPTER 1

INTRODUCTION

1.1 Research Background

The transportation sector accounts for about 25 % of energy consumption over the world (Jean-Paul Rodrigue, 2020). Rail, being one of the most energy-efficient transport modes, features a far lower energy intensity and carbon emission as compared with that of other transport modes. The report from International Energy Agency has shown that rail services account for 9 % of global motorised passenger movement and 7 % of freight, but with only 0.3 % of direct carbon dioxide (CO₂) emissions and 3 % of transport energy use (International Energy Agency, 2020a).

Conventional diesel-driven trains have been gradually superseded by electrified trains due to their low energy efficiency, high carbon emission, and high operation and maintenance costs (García-olivares, Solé and Osychenko, 2018). Investment in railway electrification has been increasing in the past decades. As shown in Figure 1.1, nearly three-quarters of the existing rail track length in the world are electrified, while the remaining quarter relies on diesel (International Energy Agency, 2020). The transition of the railway industry from diesel-driven to electrification is one of the solutions to the challenge of sustainable development and fundamental to achieving global energy transition.

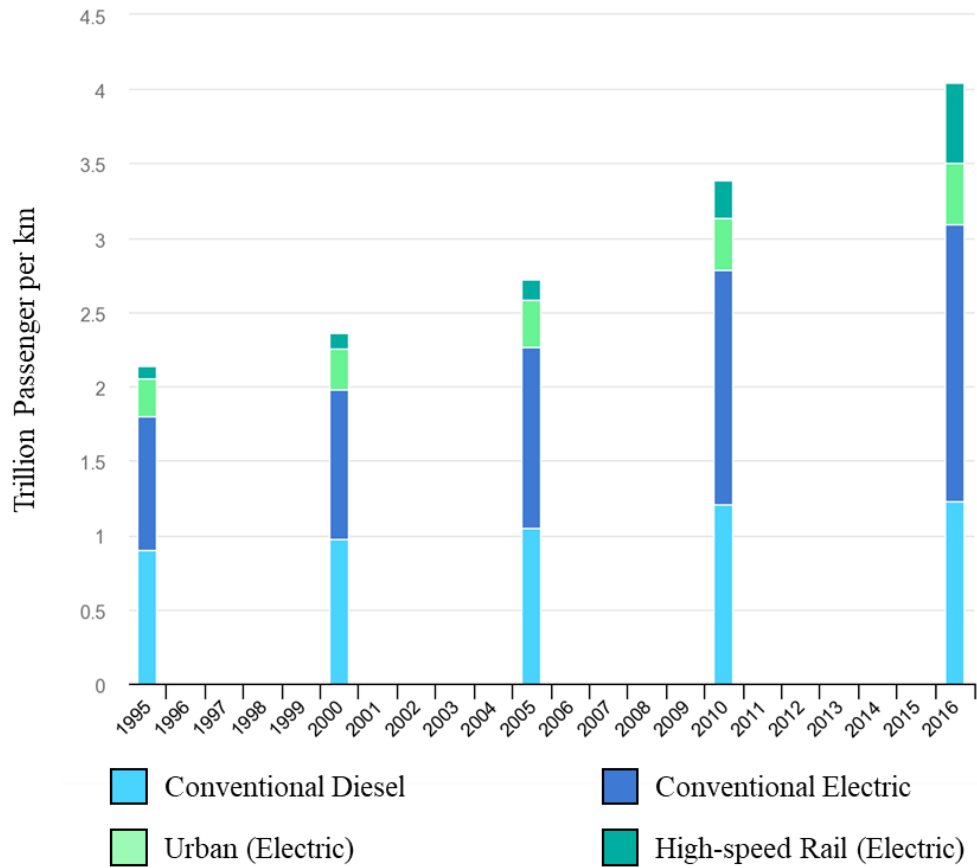


Figure 1.1 Passenger rail transport activity by fuel type from the year 1995-2016

Despite being one of the most energy efficient transportation modes, the rail transport system still consumes a large amount of energy. A report from the International Energy Agency has shown that the total energy consumption for global rail services in the year 2019 is around 280 TWh of electricity (International Energy Agency, 2020). Hence, the energy cost is one of the largest expenses for railway companies. Improving the energy efficiency of railway systems is still the main interest for these companies to reduce energy consumption as well as the operating cost (Fernández-rodríguez *et al.*, 2015; Su, Tang and Wang, 2016).

Electrified trains are usually supplied either through the AC overhead catenary system or through the conductors called the third rail that is fed by a DC supply. The third rail DC traction power system is economic for modern urban transportation that features a low voltage, high passenger capacity, and low speed (Chymera and Goodman, 2006; Cantor *et al.*, 2012). A typical third rail DC railway system is supplied from bulk supply substations (BSS) where the intake is a high voltage at 132 kV.

The main transformers in the BSS play an important role in maintaining the reliability of the railway traction power systems in the event of an electrical failure or an unexpected shutdown. Hence, the railway traction power systems are usually designed with additional power transformers in the main-tie-main configuration. In the event of one transformer outage, the affected loads can be immediately supplied by the other transformers.

There are three BSS transformer operation modes for main-tie-main configuration, namely non-parallel operation, parallel operation, and single transformer mode. Different operation mode results in different transformer demand profile and overall loading level, which leads to different transformer power losses. Unnecessary power losses can be avoided if the BSS transformers operate at the optimal operation mode with the lowest power losses.

The railway system is relatively complex as compared to other conventional distribution networks due to its inherent dynamic characteristics. Train movement can be categorised into 4 main phases, namely, acceleration, cruising, coasting, and braking phases. These movement phases result in time-varying characteristics of the traction loads. Track parameters such as gradient, curves, speed limit restrictions, and tunnels that have different aerodynamic resistances increase the complexity of the train's dynamic characteristics. These factors make the operations of a traction network being different from the normal distribution network.

Due to the fact that the traction loads are inherently dynamic, the approaches to search for the optimal transformer mode in railway systems are not as straightforward as that of industrial and commercial distribution networks. In this research, a comprehensive simulation model for an urban rail transportation system is developed. The simulation model comprises both the low voltage traction network and high voltage supply network of the railway system. The dynamic characteristics of the low voltage traction network are derived from the train movement and track conditions. The dynamic traction load from the low voltage traction network is connected to the high voltage supply network, thus allowing the high voltage network to be analysed dynamically.

Power adequacy study is essential for the design stage of a railway system. The power system must be capable to supply all the loads in steady states under

standard conditions. In a power adequacy study, the power supply network must fulfil two requirements:

- The ability of the connected utility grid to cover the maximum load under various generation availability and load level conditions, taking into account the possible uncertainties.
- The ability of the transmission system to perform while maintaining the flexibility provided by interconnections.

In common practice, power adequacy studies are done by performing power flow analysis on the worst-case scenarios, to investigate the maximum capability of the power system. On the other hand, dynamic analyses are performed in this research to investigate the impacts of traction dynamics on both the low voltage traction network and high voltage supply network. Power flow is done on each time step, to expand the calculated results in the time-domain. With the dynamic analyses, the railway system is analysed, not limited to worst-case scenarios, but with various traction load conditions. Therefore, dynamic analyses can investigate the supply capability of the railway system at peak load, as well as accurately determine the energy consumption and power losses of the railway system.

The energy efficiency of the railway system can be improved by implementing the optimal BSS transformer operation mode at respective train headway intervals. The optimal operation mode of the BSS transformers can be found if an operation mode with the lowest transformer power losses is determined. In

this research, dynamic analyses are essential to achieve an accurate estimation of BSS transformer power losses in various scenarios. By using train schedules with different headway intervals, the variation on the low voltage traction load is created. For each headway interval, dynamic power flow simulations with different BSS transformer operation modes are performed.

However, each operation mode has its unique drawbacks and challenges that might cause inefficiency in the power system. Hence, the advantages and disadvantages of isolated transformer operation and parallel transformer operation are studied in this research. Short-circuit studies are done on the high voltage supply network of the railway system to investigate the negative impacts of parallel transformer operation on the protection of the power system.

1.2 Research objectives

The objectives of this research work are as follow:

1. To develop dynamic traction load models for railway power supply network.
2. To perform dynamic analyses on the railway system.
3. To evaluate the optimal operation mode of the transformers with different train schedules with the final aim of achieving power loss reduction.

4. To observe the impact of parallel transformer operation on the short-circuit current of a railway system.

1.3 Scope of research

This research proposed an approach for the optimal operations of the BSS transformers in railway systems. The optimal operation mode can be found if the operation mode has the lowest transformer power losses. To accurately determine the power losses, a comprehensive electrical model that comprises of the low voltage traction network and high voltage supply network of a railway system was developed using ETAP-Etrax software. The technical parameters for the power system and rolling stocks are provided by the rail operator. Power adequacy studies with dynamic power flow analyses were done on the railway model. The simulations have taken into account the train dynamics and track conditions, and their impacts on the high voltage supply network. The power losses by the BSS transformers under different BSS operation modes and train headway intervals are investigated. Short-circuit studies were also done in ETAP software to observe the impact of parallel transformer operation.

1.4 Dissertation organisation

The structure of the dissertation is organised as follows:

Chapter 2 reviewed the past works on the energy saving measures in railway systems. The challenges associated with the excessive energy from regenerative braking are discussed, followed by the literature reviews on existing solutions to maximise the utilisation of regenerative energy. The benefits and challenges of implementing energy efficient driving are discussed, followed by reviews on a few works on improving driving strategies with numerical algorithms. It is followed by the literature review on parallel transformer operations in the power system. Economic benefit assessments on parallel transformer operations are also discussed.

Chapter 3 described the power system configuration of the railway system, the methodology for the simulation model development, and the considerations and assumptions included for the power adequacy studies. A detailed discussion on the design of the high voltage supply network is included together with the important parameters of the power system components. All the possible BSS transformer operation modes are introduced, and the differences between the operation modes in terms of transformer efficiency are discussed. The railway operation plans for emergency scenarios are analysed. The derivation of the formulation of transformer efficiency is discussed. A detailed discussion on the train dynamics is included under the low voltage traction network section. The parameters for rolling stocks and railway tracks are included. The calculation for dynamic power flow used by ETAP software is explained in detail, followed by the assumptions made to simplify the simulation model. The methodology, input parameters, and acceptance criteria for short-circuit studies are discussed in detail.

Chapter 4 discussed the simulation results on the low voltage traction network, high voltage supply network, BSS transformer performances, and short-circuit analyses. Power profiles and the speed profile of a single train is investigated. The differences in transformer losses between non-parallel mode, parallel mode, and single transformer mode are explained. The impact of train schedules with different headway intervals on system energy consumption is investigated. The change of BSS transformer losses for all the operation modes due to increasing headway intervals are explained. Maximum short-circuit current at 132 kV level and 33 kV level of all BSSs for all possible operation modes, in both normal scenarios and emergency scenarios, are compared in detail.

Chapter 5 concluded all the key findings and the novelty of the research. The limitations and future work on the simulation model are also elaborated.

1.5 List of Publications

The research findings have been published in peer review journals and international conferences as listed in Table 1.1.

Table 1.1 List of publications

No	Title/ Status/ Link	Status	Journal (J)/ Proceeding (P)/ Conference (C)	Index/ Impact factor
1	Optimal operations of transformers in railway systems with different transformer operation modes and different headway intervals	Published	(J): International Journal of Electrical Power and Energy Systems	ISI / 3.588
2	Short-Circuit Analyses of Parallel and Non-Parallel Transformer Operations for Railway Power Supply: A Case Study for Third Rail System	Published	(P): 2020 (8 th) International Conference on Smart Grid and Clean Energy Technologies	SCOPUS

CHAPTER 2

LITERATURE REVIEW

2.1 DC Traction Power Systems

Typical standard voltages worldwide for the third rail DC system are 600 V and 750 V (Srivastava, Kumar Singh and Singhal, 2013; White, 2015; Kampeerawat and Koseki, 2017; Zaboli *et al.*, 2017). However, there are a few railway systems that adopt non-standard system voltages such as 1200 V and 1500 V (Knesebeck, 2011; Srivastava, Kumar Singh and Singhal, 2013; Lin, Song and Feng, 2014). Current DC railway systems are limited to low catenary voltage due to the blocking voltage issues of the semiconductors (Serrano-Jiménez *et al.*, 2017). Thus, the locomotive power and traffic density in DC railway systems are limited to prevent high currents flowing in the conducting line (Palacin, Batty and Powell, 2014). As a result, current DC railway systems are economically beneficial for low-speed applications. However, recent development in semiconductor technologies has made higher DC voltage railway systems feasible. Verdicchio *et al.* proposed a strategy to upgrade an existing 1.5 kV DC railway system to 9 kV DC (Verdicchio *et al.*, 2019).

2.2 Energy Saving on Railway Systems

Industrial and academic researchers have been finding new solutions to reduce the energy usage of the railway systems, with the aims of reducing carbon emission and cut down the energy cost. In recent decades, there are three main approaches to increase the energy efficiency of the train systems, namely the implementation of regenerative braking, implementation of energy efficient driving, and loss reduction on the supply network and its components.

2.2.1 Regenerative Braking

Regenerative braking refers to an energy recovery mechanism that converts kinetic energy from a moving vehicle into a form that can be reused later, typically electricity. Regenerative braking has become common in commercial urban rail systems in past decades and has reduced the system's net energy consumption between 10% and 45%, depending on the characteristics of each system (González-Gil, Palacin and Batty, 2013). However, managing the regenerated energy has been the main challenge (Kampeerawat and Koseki, 2017). This issue is especially crucial in DC railway systems because they are not receptive (Almaksour *et al.*, 2020).

Generally, the recovered energy is only usable when there is a simultaneous consumption, for instance when there is another accelerating train. Otherwise, the excess energy that is not used within the system is converted into heat using

a dedicated resistor bank (Roch-dupré *et al.*, 2021). This implies that the energy is wasted, and it will cause cooling issues, induce additional weight, and increase costs (Lin, Song and Feng, 2014). The popular solutions in existing systems for the aforementioned issues include timetable optimisation, installation of an energy storage system (ESS), and increasing receptivity of the system.

2.2.1.1 Increasing Receptivity of DC Railway System

The most fundamental approach to maximise the utilisation of regenerative braking in railway systems is to allow the recovered energy to supply to other components connected to the power supply network. While AC railway systems are naturally receptive, DC railway systems generally do not allow power flow reversely from vehicles to the supply network, due to the commonly used diode rectifier as AC-DC converter, which is unidirectional. The solution to increasing the receptivity of DC railway systems includes the use of additional inverters in a substation. However, this induces costs for the rail operators, and it requires robust control for the inverter operations (Ceraolo *et al.*, 2018).

Almaksour *et al.* proposed a simulation model to investigate an addition of a controllable inverter that makes an existing substation of a DC railway system reversible (Almaksour *et al.*, 2020). The proposed control strategy for the inverter is based on the voltage level of the catenary. Comparison between the configuration of the simulation model with or without inverters shows an energy consumption reduction of the system up to 6.9 %. The proposed simulation

model is validated by comparing it with the results obtained from a professional software called Esmeralda.

Another research to transform existing DC railway substations from unidirectional to reversible with the installation of an inverter has been done (Cornic, 2010). In this study, the rectifier operates only in normal mode where the substation supplies power to the catenary, while the newly installed inverter operates in both normal mode and recovery mode. In normal mode, the inverter operates as an active filter to mitigate voltage fluctuation and harmonic distortion, while in recovery mode, the inverter provides a path for the recovered energy to flow back to the AC power supply network. Results showed annual energy saving up to 18 % of the initial energy consumption of the substation, and demonstrated the feasibility of removing the on-board braking resistors.

2.2.1.2 Timetable Optimisation

Timetable optimisation is the approach to coordinate the accelerating and braking action of trains so that the recovered energy from the braking train can be immediately used by the accelerating train. Figure 2.1 illustrates the concept of timetable optimisation to improve the utilisation of regenerative energy. The overlapping area denoted by the grey triangle in the figure is the amount of utilised regenerative energy. From the figure, Profile 2 of train i is the result of left-shifted Profile 1, indicating that profile 2 has an earlier train departure time. Profile 2 of train i achieves a larger overlapping area with the profile of train j than that of profile 1. By finding the optimal arrival and departure time of the

vehicles, the overlapping area can be enlarged, resulting in maximising the utilisation of regenerative energy (Yang *et al.*, 2016). However, this approach reduces the flexibility for timetable planning and is ineffective for systems with a frequent event of trains deviating from the scheduled timetable due to some uncertain and stochastic factors (Qu *et al.*, 2020)

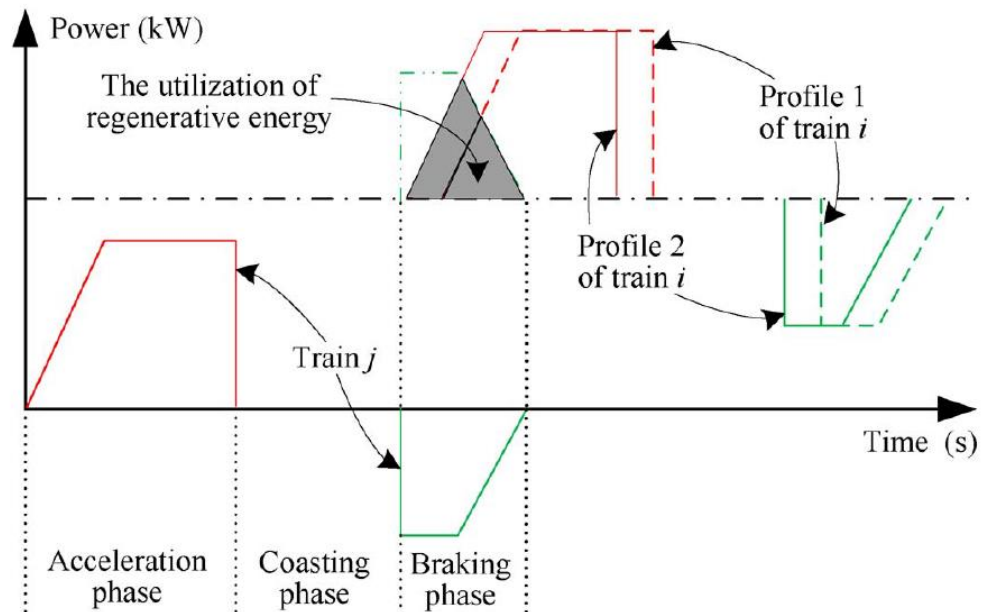


Figure 2.1 Utilisation of regenerative energy from the power-time profile of two trains

Yang *et al.* proposed a timetable optimisation model to maximise the utilisation of regenerative energy, while at the same time reduce the passenger waiting time (Yang *et al.*, 2014). A two-objective integer programming model that includes train dwell time and headway time control has been formulated. The optimal solution is found by implementing a genetic algorithm with binary encoding. The proposed model achieved a reduction of energy consumption up to 8.86%,

and a reduction of passenger waiting time up to 3.22 %, tested with actual operation data from the Beijing Yizhuang subway line in China.

Liu et al. proposed a new timetable optimisation problem that includes the consideration of realistic constraints with the decision variables, such as train dwell time and headway interval, to maximise the utilisation of regenerative energy (Liu *et al.*, 2019). The optimisation problem is solved using an Improved Artificial Bee Colony (IABC) heuristic algorithm. The mathematical model is tested with actual operation data from the Yanfang subway line in Beijing, China. The efficiency of the IABC algorithm is proved by comparing it with the genetic algorithm and a commercial software named CPLEX. The result concludes that the REU improvement ratio of 34.7 % can be achieved by optimising both the dwell time and headway time.

2.2.1.3 Energy Storage Systems in Railway

In recent years, the installation of energy storage systems (ESS) in a railway system has become a popular alternative to manage the regenerated energy from the trains. By temporarily storing the regenerated energy in the ESS, the energy can be used without restrictions by the timetable. Further advantages of the ESS are voltage stabilisation, reducing peak power demand of the traction substations, and emergency supply (Meishner and Sauer, 2019). However, the number and the sizing of ESS are usually restricted by the high cost of the ESS itself. A robust control strategy is essentially important to ensure the performance and reliability of the ESS, which in turn, induces a high cost to the rail operator. An

ESS that is installed onboard a train causes an increase of train weight, resulting in lower energy efficiency of the vehicle.

Generally, the ESS can be installed onboard the train (Arboleya and Armendariz, 2016), or at the wayside along the track (Alfieri, Battistelli and Pagano, 2019). The types of ESS that are most commonly used include batteries (Kumar *et al.*, 2012), supercapacitor (Teymourfar *et al.*, 2012), and flywheel (Lee *et al.*, 2013).

Energy storage systems that are installed on-board a train are called On-board ESS (OBESS). OBESS stores the recovered energy of only one train, thus the required capacity is lower. Nonetheless, the capacity must be able to satisfy the energy demand and peak power generated by the train during the braking phase. The main objective of the control strategies for OBESS is to reduce the peak current of the train during the acceleration and braking phase, flowing to and from the contact line.

The strategy more frequently used in OBESS is to suppress the maximum current that a train draws from the contact line during acceleration or returns to the contact line during regenerative braking (Ogasa and Taguchi, 2007). Takagi *et al.* proposed a control strategy for the charging and discharging of OBESS on a DC railway system based on the feed-forward data (Takagi and Amano, 2015). The feed-forward data is the reference state-of-charge (SOC) curve which is pre-calculated data to determine the desirable SOC of the ESS at a certain train position. The trajectory of charging and discharging of the OBESS is determined

based on the trajectory of traction power. The proposed control strategy was validated by performing a simulation based on an existing railway in Japan.

Energy storage systems that are installed on a fixed location are called Stationary ESS (SESS). The stationary storage system is typically installed on the wayside of along the rail line, hence is often called Wayside ESS (WESS). Different from OBESS, a WESS interacts with all the trains passing by the location, either to store the energy recovered from the braking, or to provide energy for acceleration. Compared to OBESS, a WESS does not have spatial limitations on sizing, therefore can provide higher energy capacity and higher power (Ghaviha *et al.*, 2017). The control strategies of WESS are typically based on line voltage (Konishi and Tobita, 2012).

Alfieri *et al.* proposed a model of a railway system with a WESS (Alfieri, Battistelli and Pagano, 2019). The impact of the WESS on the power flow within the entire infrastructure is examined. Dynamic analyses that considered the position and speed of moving trains, as well as the track parameters, are implemented. The impact of the WESS is evaluated in terms of energy efficiency and power quality, particularly the voltage profile curves.

The installation of a WESS in a railway system is crucial to achieving the optimised battery sizing and locations while maintaining the investment cost at a reasonable level. The performance of three heuristic algorithms, namely genetic algorithm, the Particle Swarm Optimisation (PSO), and the Fireworks

Algorithm (FA) in optimisation work for the installation of WESS on a railway system are compared (Roch-dupré *et al.*, 2021). The results showed that the genetic algorithm has the best performance with the fastest speed of convergence, followed by FA and PSO.

Ratniyomchai *et al.* proposed a nonlinear mathematical optimisation model based on Lagrange multipliers (LGM) to search for optimal size and location of the supercapacitor-based ESS (Ratniyomchai, Hillmansen and Tricoli, 2014). The results showed that the smallest available capacity of the superconductor based ESS can be obtained when the ESS is installed near a substation. The results also showed an energy consumption reduction of up to 63 % during the acceleration phase of a train, verified using a single train simulation model.

The types of ESS that are most commonly used include batteries (Kumar *et al.*, 2012), supercapacitor (Teymourfar *et al.*, 2012), and flywheel (Lee *et al.*, 2013). The advantages of a battery type ESS include fewer voltage fluctuations, low self-discharge rates, and high energy capacity. Thus, a battery type ESS is more suitable for a WESS than an OBESS. WESS with Lithium-ion batteries and Nickel-metal hybrid batteries are commonly used in railway systems (Ghaviha *et al.*, 2017). Supercapacitors are also widely used in existing state-of-the-art railway systems due to their high charging and discharging capability, long life span, and maintenance-free characteristics. Thus, supercapacitors are more suitable to be used in OBESS for power demanding (Ghaviha *et al.*, 2017). Experimental results from a light rail system with on-board supercapacitors in

Germany shows an energy saving of 30 % (Steiner, Klohr and Pagiela, 2007), while the energy saving rate by employing supercapacitor based ESSs can be up to 35.8 % in theoretical assessment (Wu *et al.*, 2020). However, supercapacitor based ESS is not widely used in commercial due to its low energy density characteristic that leads to a high cost per MJ of energy storage (Gelman, 2013). Flywheels are one of the older technologies which store energy in kinetic form, via the moment of inertia of a vertically or horizontally oriented rotational mass. Flywheel storage offers a high life-cycle, short response time, and low environmental impact. However, the drawbacks are the high maintenance cost and high investment cost for high-speed types (Ghaviha *et al.*, 2017). Although the application of flywheels as ESS in railway systems has been developed a long time ago (Okui *et al.*, 2010), the approach of using flywheel in an OBESS is still at the early development stage (Wu *et al.*, 2020).

2.2.2 Energy Efficient Driving

Urban rail transport system conventionally adopts maximum speed driving strategy for its simplified control system and schedule management. However, such driving strategy is not energy efficient. Hence, energy efficient driving is one of the current research trends to improve the efficiency of the traction loads in railway systems. The main purpose of energy efficient driving is to find a speed profile with minimum energy consumption. Reducing the maximum speed and increasing coasting are two efficient means of saving energy. The cost of doing so is an increase in travel time, which has to be avoided because passenger travelling time is valuable. Figure 2.2 shows the relationship between train travel

time and minimum energy consumption available by the vehicle (Yang *et al.*, 2016). To achieve the maximisation of social welfare, the optimal coasting speed of train sets between stations should be determined by considering the cost of the passenger traveling time and the cost of propulsion energy of the train set.

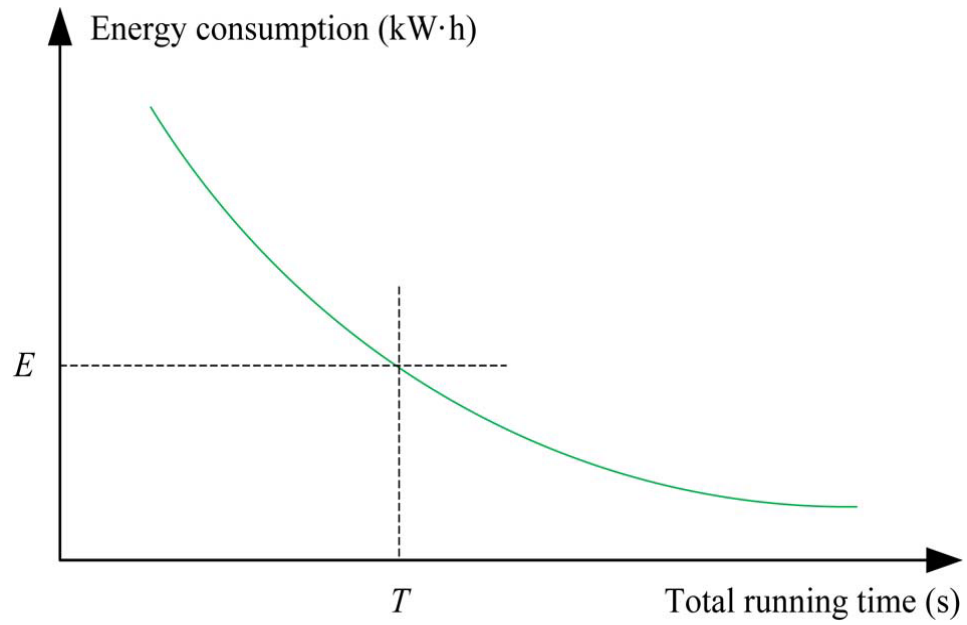


Figure 2.2 Relationship between train travel time and minimum energy consumption (Yang *et al.*, 2016)

An optimal control model is first proposed in 1968 to determine the energy efficient speed profile (Yang *et al.*, 2016). In recent years, with the development of computer performance and calculation theory, numerical algorithms such as genetic algorithms, dynamic programming are involved in more and more researches on energy-efficient driving. The optimisation model becomes more complicated considering more real-world conditions, such as varying gradients, arbitrary speed limits, and different radius curves (Yang *et al.*, 2016).

Chang et al. proposed an artificial neural network (ANN) to determine the optimal coasting speed of the train set for a mass rapid transit (Chuang *et al.*, 2008). The objective function is formulated by considering the cost of energy consumption and the cost of the passenger traveling time. The proposed algorithm has been tested out in a simulation using real-time data of the Kaohsiung MRT system, together with forecast data of passenger ridership.

A comparative study between Genetic Algorithm (GA), Ant Colony Optimisation (ACO) and Dynamic Programming (DP) on energy efficient driving has been done (Lu *et al.*, 2013). A distance-based train trajectory searching approach has been used, where the model obtains the speed level at each position instead of searching for a detailed complicated control input for the train traction system. It was found that DP performed better than both GA and ACO.

Su et al. proposed a few strategies to improve the coordination between high level and low level control of the automatic train operation (ATO) to achieve energy-efficient driving (Su *et al.*, 2014). The proposed strategies include expanding the tolerable speed error, setting a smart target speed, and the combination of both. The proposed strategies are capable of avoiding unnecessary switching and then efficiently reduces the traction energy consumption of the train switches. The proposed approach is tested out via simulation using real data of the Beijing Yizhuang rail transit line.

Domínguez et al. proposed an efficient MOPSO algorithm to cope with new signalling technology (Domínguez *et al.*, 2014). The signalling technology permits a better bandwidth allows more detailed control of the vehicle speed, thereby improving the energy efficient driving of the trains. The algorithm has been used to obtain the optimal speed profiles in a real line of the Madrid Underground. The algorithm is also able to take into account only the speed profile that is comfortable to passengers.

2.2.3 Loss Reduction on Supply Network

Another approach to achieve energy saving in railway systems is to reduce the energy losses generated in the power supply network. As the resistive losses in the power supply network are a quadratic function of the current, implementing the rail operations in higher electrification voltage is one way to minimise the energy losses (Palacin, Batty and Powell, 2014). Other options are usually based on the deployment of improved materials. However, both aforementioned approaches usually imply a large number of investment costs.

Tomita et al. completed the development of a prototype of High-Temperature Superconducting (HTSC) DC cable that is ideal for a feeder of the overhead contact line system (Tomita *et al.*, 2010). The authors foresee that with the use of superconducting cable, the voltage drop would be significantly reduced, leading to a decrease in the required number of substations. However, the

product is yet to be ready for mass production, and the economic feasibility of replacing current copper wires with the product is not discussed.

Fabre et al. provided guidelines for a full silicon carbide (SiC) inverter design in railway systems (Fabre, Ladoux and Piton, 2015). The advantages of SiC technology in terms of blocking voltage, operating temperature, and switching speed are evaluated. The experimental results have shown that SiC-MOSFET devices achieved a significant loss reduction compared to conventional Si-IGBT devices. However, the cost of this technology was not discussed.

2.3 Parallel Transformer Operation

Parallel transformer operation has been commonly implemented in conventional power system. The works of literature by Huang et al. and Jaramillo et al. summarised the positive impacts brought by parallel transformer operation (Huang *et al.*, 2014; Jaramillo-Duque *et al.*, 2018). With parallel connected transformers, it is possible to switch off one of them while avoiding any undesired loss of load for maintenance purposes, thus increasing the availability of the power system. Similarly, the system reliability is increased, as the operation of the power system will not be interrupted when there is an outage of one of the transformers. In addition, parallel transformer operation provides flexibility to the power system to cope with the demand growth, as new transformers can be installed parallelly to the existing transformers.

However, the challenges of implementing parallel transformer operation are the flow of circulating current in between the transformers (Chen *et al.*, 2016; Jaramillo-Duque *et al.*, 2018), synchronisation of tap changers (IEEE Standards Association, 2015), and increases of fault level at the secondary side of the transformers.

Jaramillo et al. addressed the circulating current problem that is caused by unbalanced voltages in the secondary sides of the transformers with different construction features (Jaramillo-Duque *et al.*, 2018). Circulating current should be avoided to prevent undesired heat dissipation and increase of internal power losses. Hence, to mitigate circulating current, the selection of transformers for parallel operation is important, and must satisfy the following conditions (Huang *et al.*, 2014):

1. The polarities of the transformers must be the same.
2. The transformers must have the same phase angle shift and phase sequence.
3. The transformers should have the same voltage and turn ratio.
4. The capacity ratio of the transformers is universally less than 3:1.

The tap changer synchronisation problem in parallel transformer operation is addressed (IEEE Standards Association, 2015). The timing differences between the tap changing of both the transformers would cause tap position mismatch. The voltage regulating mechanism of the second tap changer would not operate

due to the half-regulated voltage done by the first tap changer. The consequences are the tap position-induced circulating current, and having the different duties on the mechanisms and mechanism contacts between both the transformers.

If both the transformers connected in parallel are not identical, the percentage impedance deviation between the transformers cannot be avoided. Jauch discussed the general approaches to improve the performance of tap changers in parallel connected transformers (Jauch, 2006). Other than the simple master-follower schemes, the tap changers can be operated in possible ways that are able to limit the flow of reactance power, to maintain equal power factors in the transformers, and to minimise circulating current. Jaramillo et al. proposed to apply a genetic algorithm to search for the optimised tap position of the transformers, with the aim of minimising the power losses generated by the circulating current (Jaramillo-Duque *et al.*, 2018). Chen et al. proposed the tap stagger operation, whereby the parallel connected transformers are purposely left with small offset tap positions, to absorb some of the reactive power, thereby achieving voltage regulation in the power system (Chen *et al.*, 2016).

One benefit of parallel transformer operation that is often neglected by researchers is the potential of power loss reduction by the parallel connected transformers. Borge et al. carried out an economic benefits assessment by implementing a parallel transformer operation for industrial and commercial loads (Borge-Diez *et al.*, 2013). A method named Parallel Losses Optimisation (PLO) is proposed to perform decision making on the configuration of a pair of

transformers, whether to be isolated or connected in parallel, based on the connected load level. A PLO Point is introduced, at which it is the lowest transformer loading level that would benefit from the parallel transformer operation, have a lower energy loss than the isolated operation. Figure 2.3 shows the PLO point of two transformers with different power ratings. The system exhibits a lower total loss if isolated transformer operation is implemented at a loading level less than the PLO point, and vice versa. The proposed strategy has made a loss reduction of up to 41 % for parallel transformer operation, validated in 12 real facilities of different power ratings and efficiency levels.

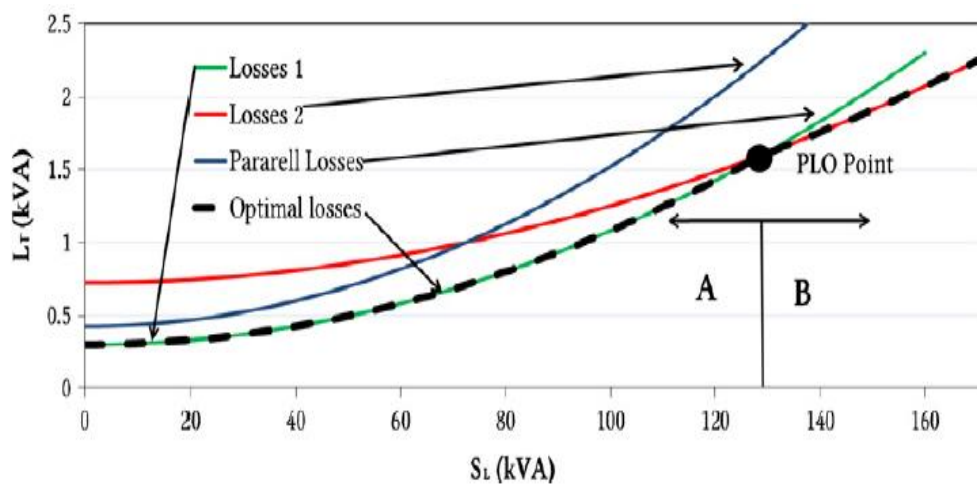


Figure 2.3 PLO point of two transformers with different power ratings (Borge-Diez *et al.*, 2013)

Jakus and Vasilj proposed a novel optimisation algorithm to determine the optimal transformer substation topologies from time to time (Jakus and Vasilj, 2018). The main objectives of the algorithm are to minimise annual energy losses, at the same time avoiding frequent transformer switching. The authors proposed

two different approaches for the algorithm. The first approach is a one-binary mathematical model that minimises the number of changes in transformer substation topology based on the constraints related to the transformer minimum up-time and down-time. The second approach is a three-binary mathematical model that imposes a limit to the maximum number of topology changes on an annual scale. The investigated substation consists of three transformers connected in parallel, resulting in 14 feasible transformer operating modes. An approximate 14.4 % reduction of annual power losses in a real substation was achieved. The proposed algorithms are particularly effective for parallel connected transformers with different power ratings and percentage impedance. However, the proposed algorithms optimise the system on an annual scale, with a sampling resolution of one hour. Thus, it is not suitable for micro-adjustment of the substation that requires a faster response time, such as railway systems.

These studies have proven that the implementation of optimal transformer operations can achieve loss reductions. However, the studies are based on industrial and commercial loads, and there are only a handful of studies carried out on different transformer operations with traction loads. Due to the fact that the traction loads are inherently dynamic, the approaches to search for the optimal transformer mode are not as straightforward as that of industrial and commercial loads.

CHAPTER 3

METHODOLOGY

3.1 Introduction

MRT2 provides an urban transportation service to the population of around 2 million people stretching from Sungai Buloh to Putrajaya. The length of MRT 2 is 52.2km with 13.5km being an underground tunnel. Between Damansara Damai station and Putrajaya Sentral station, there are 26 elevated stations and 11 underground stations along the railway, hence making up a total of 37 stations.

Figure 3.1 shows the map of the MRT2 route.

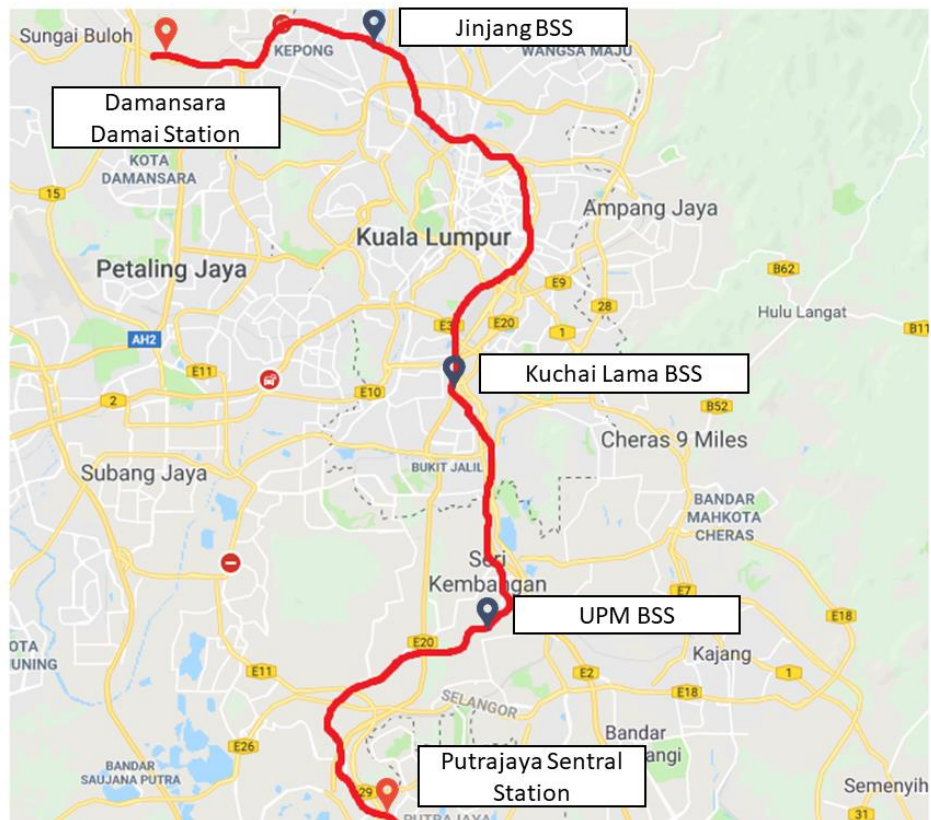
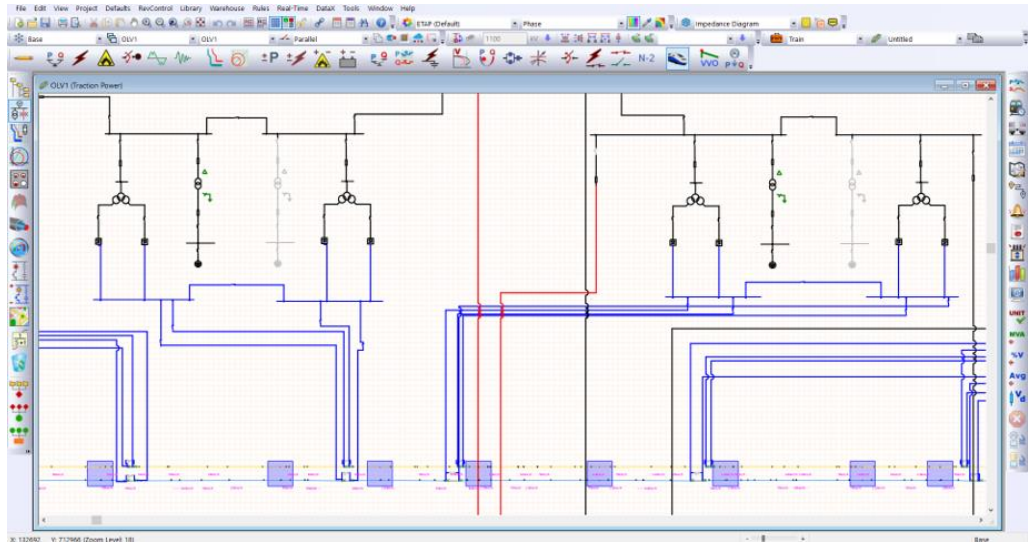


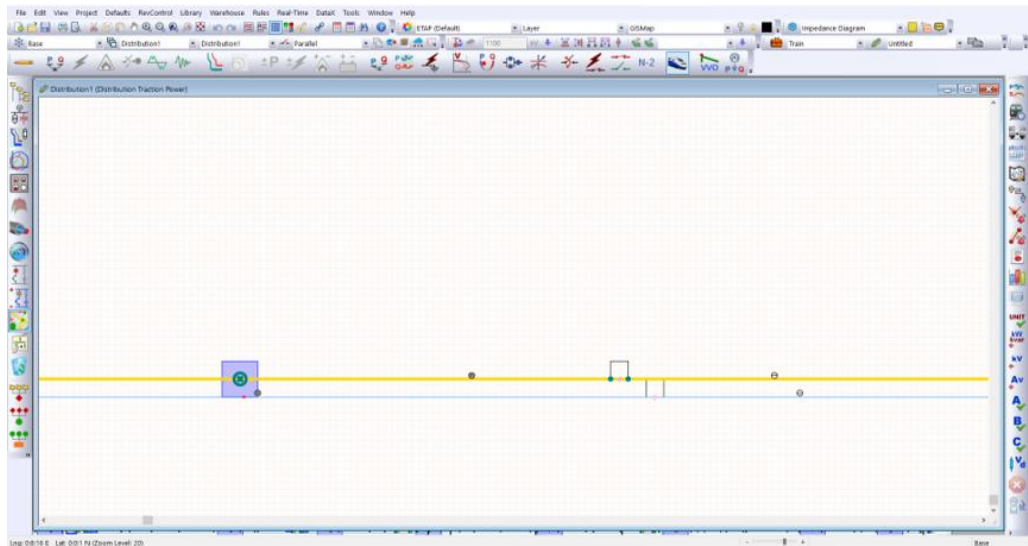
Figure 3.1 The map of the MRT2 route

The electrical network for MRT2 Malaysia has been modelled using the ETAP-Etrax software. ETAP is a professional power system software for power flow analyses and voltage drop calculations of an electrical network with a large number of buses with reliable and accurate results. ETAP has a user-friendly interface that can create, manage, and analyse the electrical networks that are visualised in the form of a one-line diagram.

The low voltage DC traction modelling of the MRT2 is done using the Etrax module of the ETAP software. Etrax is a comprehensive add-on module for simulating the impacts of train dynamics on the electrical diagram of the railway system. Etrax integrates with electrical supervisory control and data acquisition (eSCADA) to achieve real-time predictive simulation which can eliminate guess works during the analyses. Etrax visualises traction power systems with synchronised geospatial and schematic views, which provides users a lot of conveniences in performing root cause and effect analysis. Figure 3.2 shows the screenshot of schematic view and geospatial view in ETAP-Etrax software.



(a)



(b)

Figure 3.2 (a) schematic view (b) geospatial view

3.2 Modelling of the High Voltage Railway Traction Power System

There are three main infrastructures in the high voltage traction power network, namely bulk supply substations (BSS), traction power substations (TPSS), and utility buildings. The entire power demand of the MRT2 line is supplied by three BSS, which are located at Jinjang, Kuchai Lama, and UPM respectively. The BSSs then supply power to 25 TPSS, which then rectifies the supply into 750V DC to the third rail system. Railway stations and intervention shafts are either supplied directly from the nearby TPSS or the utility buildings. Table 3.1 shows the number of TPSSs and utility buildings connected to each BSS.

Table 3.1 Number of TPSS and utility building connected to each BSS

BSS	No. of TPSS	No. of Utility Building
Jinjang BSS	8	10
Kuchai Lama BSS	8	6
UPM BSS	9	5

3.2.1 Bulk Supply Substations (BSS)

The BSSs are connected to the local 132 kV grid and step down the voltage to 33 kV to form a medium voltage network before it is rectified into a DC supply by TPSSs. Both the Jinjang BSS and Kuchai Lama BSS are equipped with two 50 MVA, 132/33 kV transformers, while the UPM BSS is equipped with a pair of 40 MVA transformers. The BSSs adopt the main-tie-main configuration with

two tie breakers, in which both the high voltage sides and low voltage sides of the two transformers are interconnected by tie breakers, namely CB1 and CB2 as illustrated in Figure 3.3. CB1 and CB2 are used for the network operator to run the network in non-parallel and parallel modes. For the non-parallel mode, both the tie breakers are normally open to isolate the two transformers. During the planned or unplanned outage of one transformer, the downstream tie breaker CB2 will be closed such that the unaffected transformer can kick in to supply power to the loads served by the other transformer. For the parallel configuration, both the tie breakers are normally closed. Figure 3.3 shows the single-line diagram of a BSS with transformers in a schematic view of ETAP.

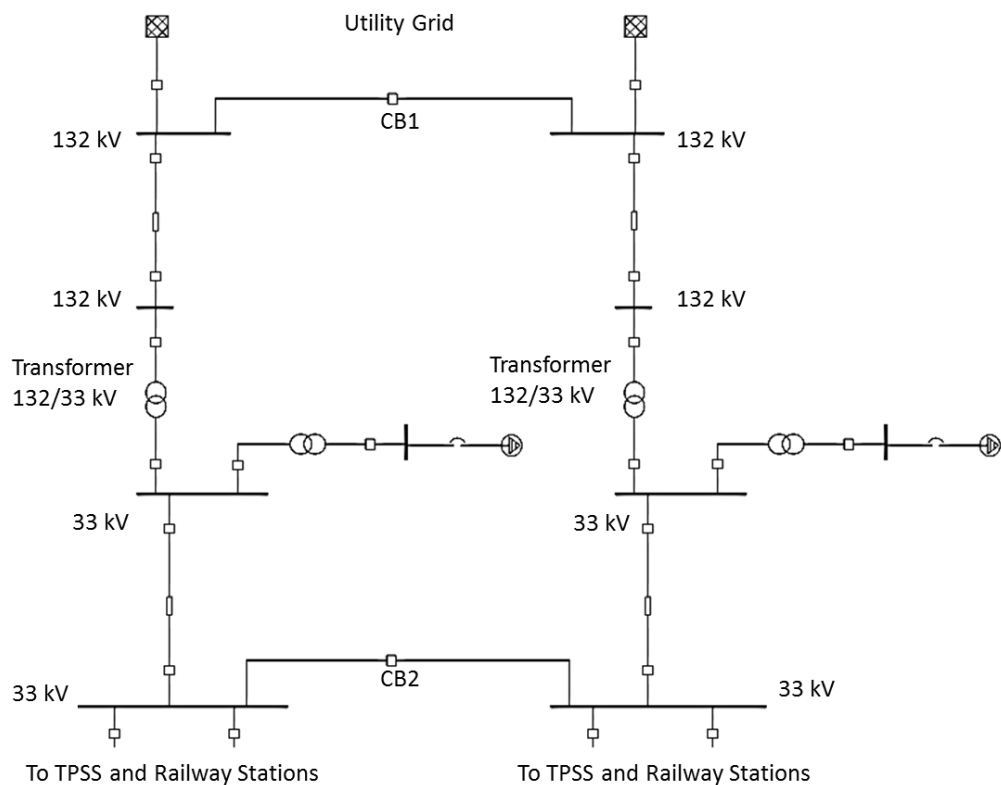


Figure 3.3 Schematic diagram of a BSS with transformers

Table 3.2 shows the key parameters of BSS transformers. These parameters are imported into ETAP software through the 2-winding Transformer Editor, as shown in Figure 3.4.

Table 3.2 Key parameters of BSS transformers

Parameters ^a	BSS Transformers	
	Jinjang BSS Kuchai Lama BSS	UPM BSS
Power Rating	50 MVA	40 MVA
Voltage level	132/33 kV	132/33 kV
Positive sequence impedance	12.5 %	12.5 %
Zero sequence impedance	10 %	10 %
X/R ratio	45	45
Impedance tolerance	±7.5 %	±7.5 %
Vector group	YNd1	YNd1

Footnotes:

a- Data collected from (Colas Rail System Engineering Sdn. Bhd., 2018b)

2-Winding Transformer Editor - JINJANG BSS TF1

Reliability		Remarks			Comment		
Info	Rating	Impedance	Tap	Grounding	Sizing	Protection	Hammonic
50 MVA ANSI Liquid-Fill Other 65 C						132	33 kV

Impedance						Z Base	
	%Z	X/R	R/X	%X	%R		
Positive	12.5	45	0.022	12.497	0.278	MVA	
Zero	10	45	0.022	9.998	0.222	50	
						Other 65	

Z Variation				Z Tolerance	
@	% Tap	%Z	% Z Variation		
-5		12.5	0	+ 7.5 %	
5		12.5	0	-	

No Load Test Data (Used for Unbalanced Load Flow only)				
	% FLA	kW	% G	% B
Positive	0.5	30	0.06	0.496
Zero	0.5	30	0.06	0.496

Buried Delta Winding Zero Seq. Impedance Typical Value

OK Cancel

Figure 3.4 2-winding Transformer Editor in ETAP

Earthing transformers are essential to provide a ground path to the delta network of the secondary side of BSS transformers. The parameters of the earthing transformer used in this model are listed in Table 3.3.

Table 3.3 Key Parameters of earthing transformer

Parameters ^a	Value
Rating	160 kVA
Voltage level	33/0.4 kV
Positive sequence Impedance	4%
Zero sequence Impedance	4%
X/R ratio	1.5
Impedance tolerance	±10 %
Vector group	ZNyn11
Earth Fault Current limit	900 A

Footnotes:

a- Data collected from (Colas Rail System Engineering Sdn. Bhd., 2018b)

As the main intake substations for a railway system, the cables in the BSSs must have a large size to prevent significant voltage drop and cable heating issues. The cable sizing for 132 kV cables and 33 kV cables are the same for all three BSSs, while the feeder cables at 33 kV have different sizing, depending on the total amount of connected loads. Table 3.4 shows the key parameters of the cables in the BSS.

Table 3.4 Key parameters of BSS cables

Cable ^a	Voltage Rating (kV)	Sizing (mm ²)	Material
132 kV Cable	132 kV	300	Copper
33 kV Cable	33 kV	630	Copper
Feeder Cables	33 kV	300 / 500 / 630 / 800	Copper

Footnotes:

a- Data collected from (Colas Rail System Engineering Sdn. Bhd., 2018b)

3.2.2 Traction Power Substations (TPSS)

The TPSSs provide electric power to both traction loads and auxiliary loads.

Figure 3.5 shows the single-line diagram of a typical TPSS in a schematic view of ETAP.

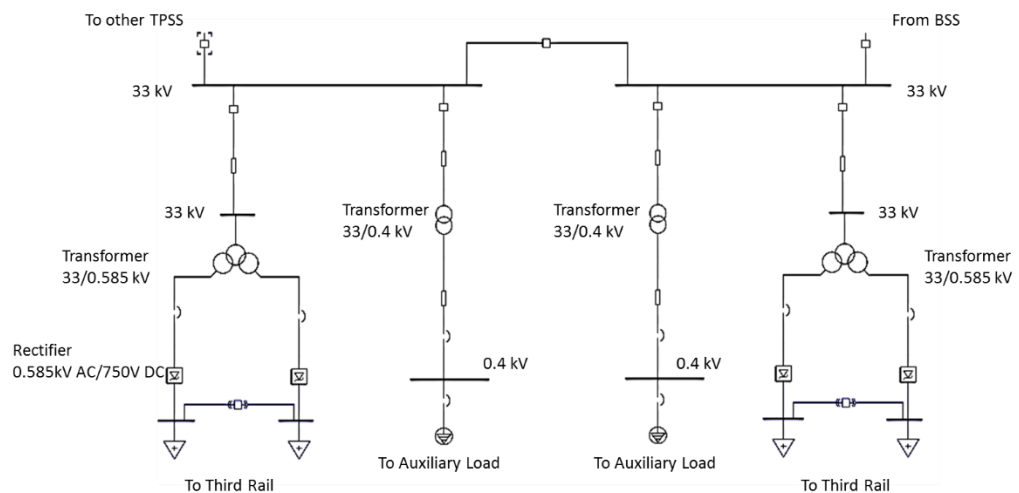


Figure 3.5 Schematic diagram of a TPSS

12-pulse rectifier models are used in the MRT2 system. The simplified rectifier model consists of a 3-winding rectifier transformer, and a pair of AC-DC converters. The rectifier transformer steps down the power supply from 33 kV

to 585 V. The rectifier transformer is an interphase transformer (IPT), in other words, the secondary windings and the tertiary windings have a phase difference of 30° as one of the efforts for harmonics mitigation. Table 3.5 shows the size and rating of the rectifier transformers. These parameters are imported into ETAP software through the 3-winding Transformer Editor, as shown in Figure 3.6.

Table 3.5 Key parameters of rectifier transformers

Parameters ^a	2.3 MVA Rectifier Transformer	3.5 MVA Rectifier Transformer
Rating	2.3/1.15/1.15 MVA	3.5/1.75/1.75 MVA
Voltage level	33/0.585/0.585 kV	33/0.585/0.585 kV
Positive sequence impedance (+Z _{pri} -Z _{sec})	6 %	6 %
Positive sequence impedance (+Z _{pri} -Z _{ter})	6 %	6 %
Positive sequence impedance (+Z _{sec} -Z _{ter})	12 %	12 %
Zero sequence impedance (+Z _{pri} -Z _{sec})	80 %	80 %
Zero sequence impedance (+Z _{pri} -Z _{ter})	80 %	80 %
Zero sequence impedance (+Z _{sec} -Z _{ter})	80 %	80 %
X/R ratio	10	10
Impedance tolerance	±10 %	±10 %
Vector group	Dd0y11	Dd0y11

Footnotes:

a- Data collected from (Colas Rail System Engineering Sdn. Bhd., 2018b)

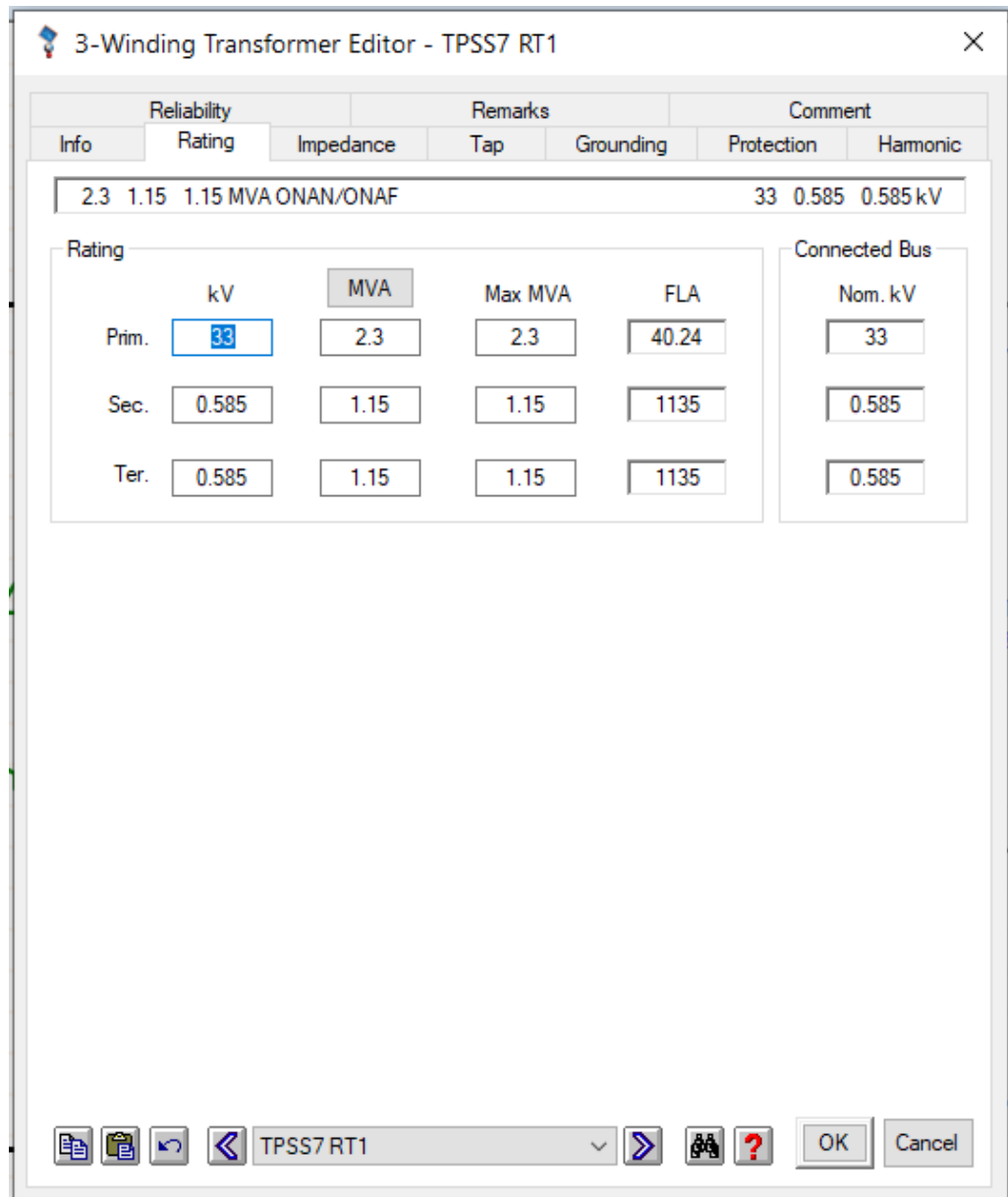


Figure 3.6 3-winding Transformer Editor in ETAP

Long cables are used to transmit power among the TPSSs. Hence, the cable sizing for a medium voltage network must be large enough to prevent significant voltage drop. Different cable sizing is used, depending on the total amount of the connected loads. The sizing of the cables connected in the medium voltage network is listed in Table 3.6.

Table 3.6 Key parameters of medium voltage network cables

Cable ^a	Voltage Rating (kV)	Sizing (mm ²)	Material
Interstation Cables	33 kV	300 / 500 / 630 / 800	Copper
Rectifier Cables	33 kV	185	Copper
MV Auxiliary Cables	33 kV	185 / 240	Copper
LV Auxiliary Cables	0.4 kV	630	Copper

Footnotes:

a- Data collected from (Colas Rail System Engineering Sdn. Bhd., 2018b)

From the low voltage side of the rectifier transformers, the AC-DC converters convert the 585 V AC supply to the 750 V DC supply that feeds the power to the rolling stocks. In this study, the default uncontrolled rectifier model in ETAP is used for the AC-DC converters. The configuration of the model is done through the AC-DC Converter Editor, as shown in Figure 3.7, with the list of parameters in Table 3.7.

Table 3.7 Key parameters for AC-DC converters

Parameters ^a	2.3 MVA Rectifier Transformer	3.5 MVA Rectifier Transformer
kW Rating	2000 kW	3000 kW
Nominal DC Voltage	750 V	750 V
Rated Continuous Direct Current	2667 A	4000 A
Nominal AC Voltage	585 V	585 V
Power Factor	0.96 lagging	0.96 lagging

Footnotes:

a- Data collected from (Colas Rail System Engineering Sdn. Bhd., 2018b)

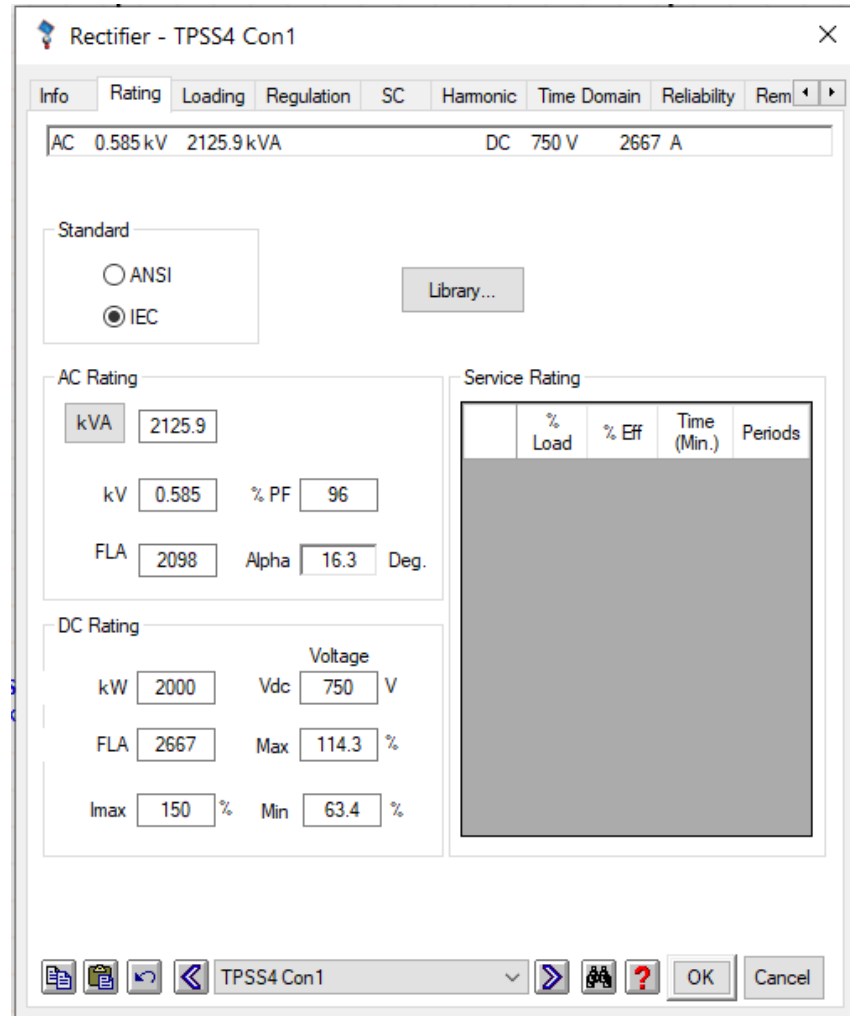


Figure 3.7 AC-DC Converter Editor in ETAP

As shown in Figure 3.5, there are two auxiliary transformers in a TPSS to supply the TPSS auxiliary loads, such as transformer cooling, circuit breaker air compressor, lightings, and control room. Some of the TPSSs also supply the nearby railway stations through the auxiliary transformers. The auxiliary transformers step down the 33 kV AC power supply to 400 V and provide power to the auxiliary loads. The TPSS auxiliary loads and the railway station loads are represented by lumped load models. The lumped loads are static models, in other

words, the power demand of the auxiliary loads is assumed to be constant at the rated power of the auxiliary transformers, with a power factor of 0.9 lagging. The auxiliary loads are also assumed as 80 % motor loads and 20 % static loads, indicating that there will be a contribution of short-circuit current from the auxiliary loads when a fault happens. The ratio of motor loads and static loads of the auxiliary loads can be configured in the Lumped Load Editor of ETAP, as ‘Constant kVA’ and ‘Constant Z’ respectively, as shown in Figure 3.8. Table 3.8 shows the key parameters of the auxiliary transformers, which are imported into ETAP through 2-winding Transformer Editor.

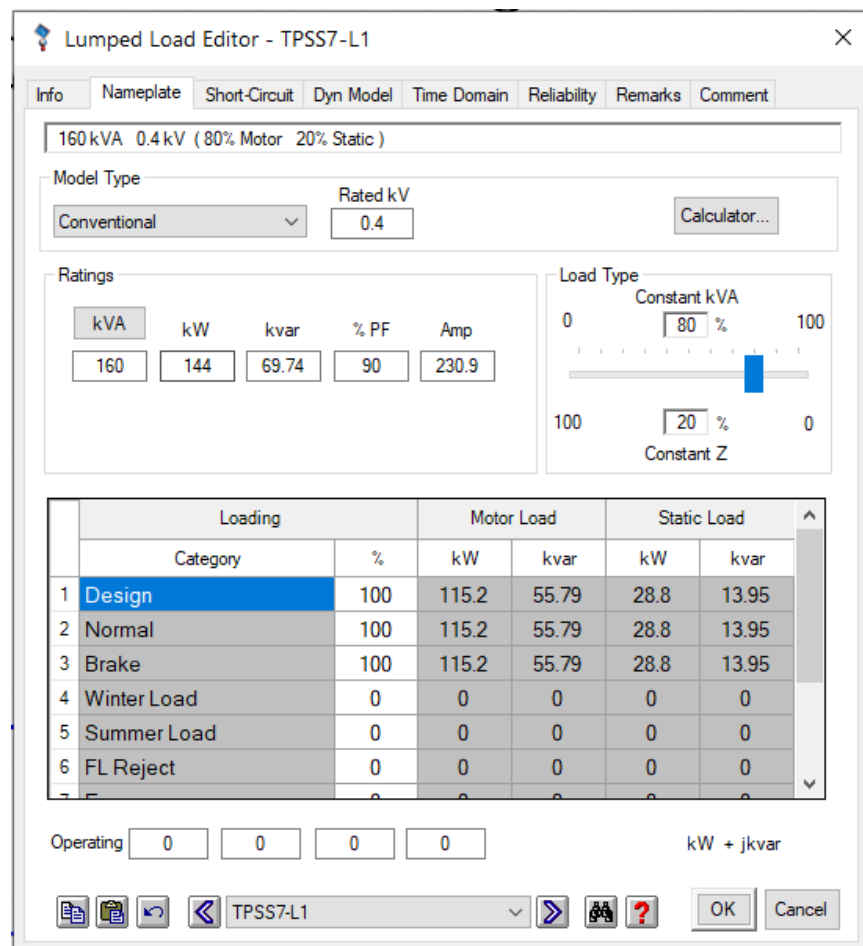


Figure 3.8 Lumped Load Editor in ETAP

Table 3.8 Key parameters of auxiliary transformers

Rating ^a (MVA)	0.16 and 0.63 MVA	0.75, 0.8, 1 and 1.25 MVA	1.5 and 2 MVA	3 and 3.15 MVA	4 MVA
Voltage level (kV)	33/0.4 kV	33/0.4 kV	33/0.4 kV	33/0.4 kV	33/0.4 kV
Positive sequence impedance	4 %	5 %	6.25 %	6.25 %	7.15 %
Zero sequence impedance	80 %	80 %	80 %	80 %	80 %
X/R ratio	1.5	3.5	6	6	8.5
Impedance tolerance	±10 %	±10 %	±10 %	±10 %	±10 %
Vector group	Dyn11	Dyn11	Dyn11	Dyn11	Dyn11

Footnotes:

a- Data collected from (Colas Rail System Engineering Sdn. Bhd., 2018b)

3.2.3 Utility Buildings

Railway stations and intervention shafts that are located far away from the TPSSs are supplied from the utility buildings. There are two 33/0.4 kV auxiliary transformers in a utility building. The parameters of the auxiliary transformers are listed previously in Table 3.8. Figure 3.9 shows the single-line diagram of the utility building in a schematic view of ETAP.

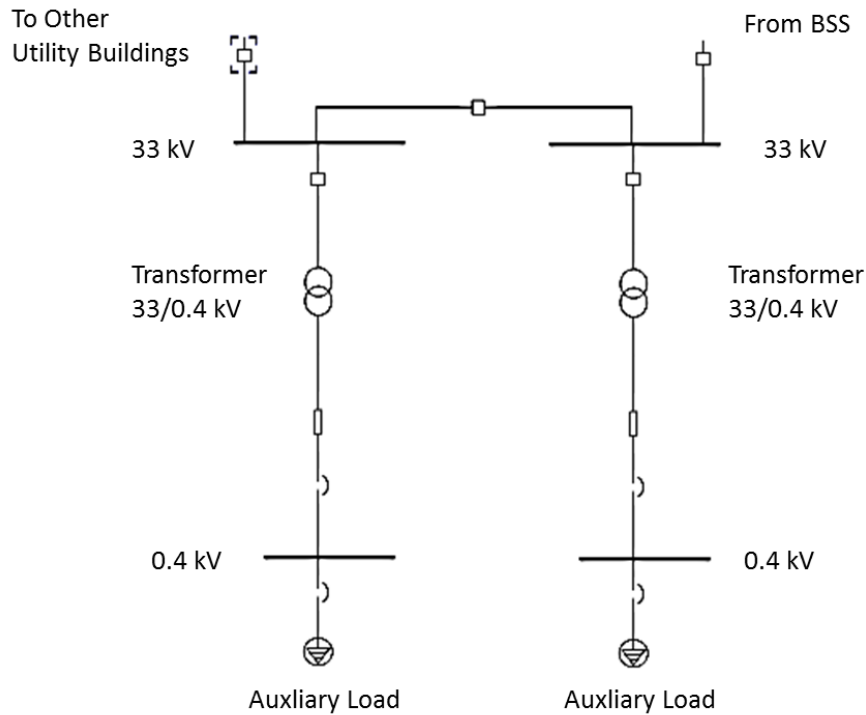


Figure 3.9 Schematic diagram of a utility building

3.3 BSS Transformers Operation Modes

There are three operation modes for BSS transformers, namely non-parallel mode, parallel mode, and single transformer mode. The non-parallel mode provides relatively simple control to the systems and a lower fault level at the secondary side of the transformers. Both the BSS transformers are isolated from each other. Due to the fact that the power demands of all the TPSSs and stations are different, therefore, the loads are not equally distributed among the two BSS transformers in non-parallel mode. As a result, the transformers may not operate at their optimal efficiency level.

On the other hand, both the BSS transformers are connected in parallel for the parallel mode. Therefore, the loads are equally distributed among the transformers, resulting in better transformer efficiency. However, the parallel mode can trigger some issues such as tap-changing synchronisation, circulating current, and high fault level to the system.

For the single transformer mode, all the TPSSs and station loads under a BSS are supplied by only one BSS transformer. The other transformer is shut down and disconnected from the network. The single transformer mode is only implemented during transformer maintenance periods and is not the main operation mode for traction power systems. Figure 3.10, Figure 3.11, and Figure 3.12 show the configuration of non-parallel mode, parallel mode, and single transformer mode, respectively.

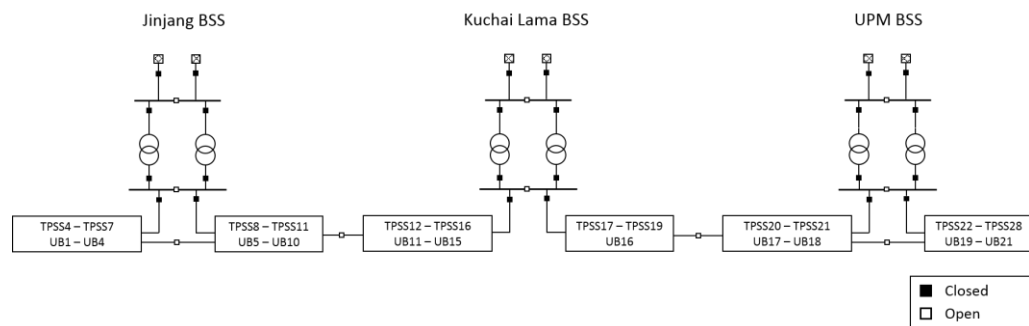


Figure 3.10 Configuration for non-parallel mode

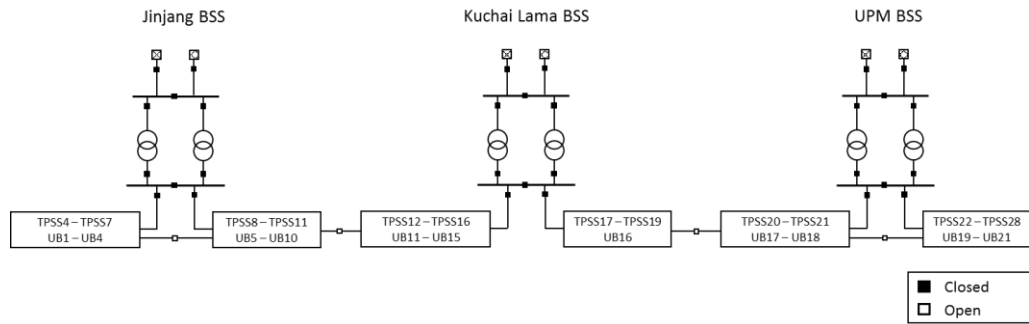


Figure 3.11 Configuration for parallel mode

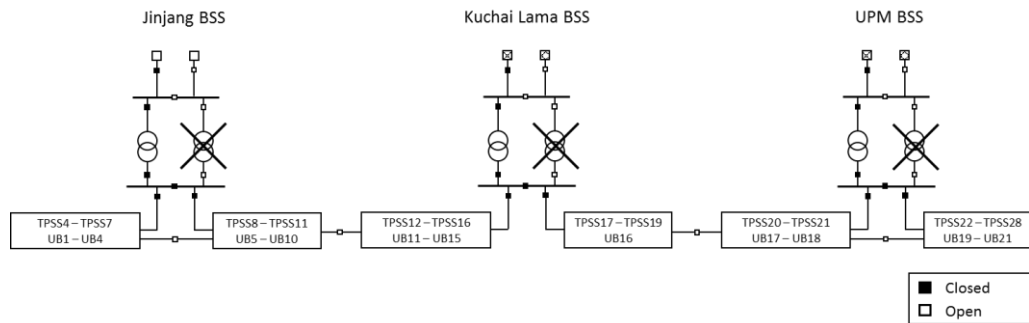


Figure 3.12 Configuration for single transformer mode

The MRT2 system operates in two possible main scenarios, namely normal scenarios and emergency scenarios. In normal scenarios, all the BSSs are segregated from each other. The BSS transformers supply to their loads in either non-parallel mode, parallel mode, or single transformer mode. On the other hand, the emergency scenario is defined as the operation failure of any of the BSS, where both the transformers in the same BSS are experiencing an outage. In this scenario, the adjacent BSS will supply power to the loads that are connected to the affected BSS. The adjacent BSS must operate in parallel mode to cope with

the larger load demand. There are three possible emergency scenarios, namely Jinjang BSS outage, Kuchai Lama outage, and UPM BSS outage.

Figure 3.13 shows the emergency scenario where the Jinjang BSS is experiencing an outage. The loads that are previously supplied by the Jinjang BSS will be supplied by the adjacent BSS, which is the Kuchai Lama BSS. The Kuchai Lama BSS will be in parallel mode, while the UPM BSS will remain to operate in non-parallel or parallel mode, as according to the normal scenario.

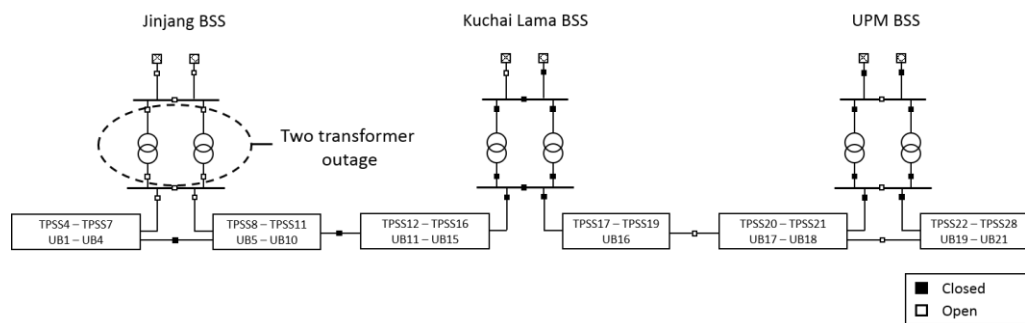


Figure 3.13 Configuration for emergency scenario (Jinjang BSS outage)

Figure 3.14 shows the emergency scenario where the Kuchai Lama BSS is experiencing an outage. In this scenario, there are two adjacent BSS involve in supplying power to the affected loads. Both the adjacent BSS will operate in parallel mode.

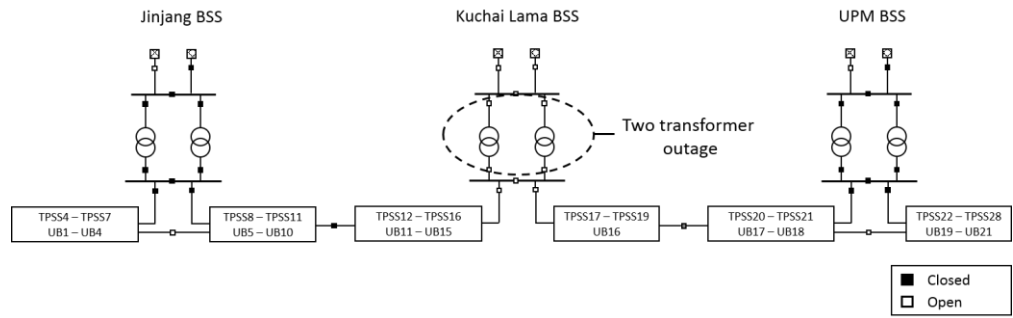


Figure 3.14 Configuration for emergency scenario (Kuchai Lama BSS outage)

Figure 3.15 shows the emergency scenario where the UPM BSS is experiencing an outage. Similar to the Jinjang BSS outage case, Kuchai Lama BSS plays the role of the adjacent BSS to supply power to the affected loads. The Kuchai Lama BSS will operate in parallel mode, while the Jinjang BSS will remain to operate in non-parallel or parallel mode, as according to the normal scenario.

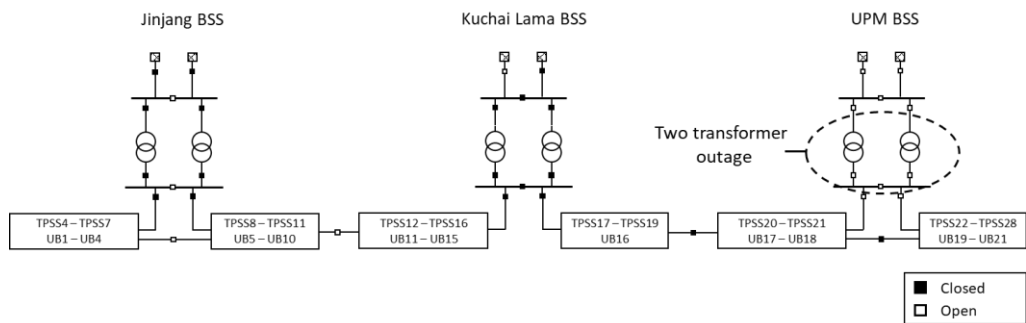


Figure 3.15 Configuration for emergency scenario (UPM BSS outage)

From Figure 3.10 to Figure 3.15, it can be seen that the operating scenarios of MRT2 are the results of states of circuit breakers. By using the Configuration Manager in ETAP, the states of circuit breakers are grouped according to the scenarios. In other words, it is not required to configure the circuit breakers one-

by-one – a single click in ETAP will change all the states of circuit breakers as in Configuration Manager. Figure 3.16 shows the user interface of the Configuration Manager that includes the states of circuit breakers for non-parallel mode, parallel mode, and single transformer mode of normal scenario.

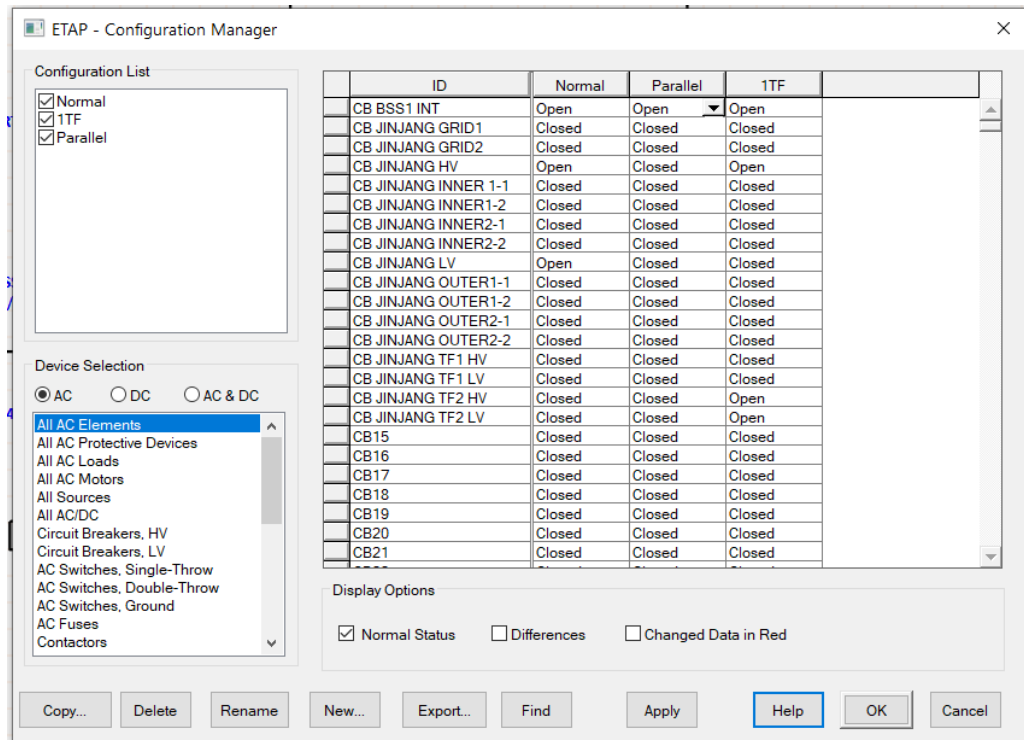


Figure 3.16 User interface of configuration manager in ETAP

3.4 Transformer Efficiency Calculations

One operation mode is considered the most optimal operation mode if it has the lowest power losses. The BSS transformer losses are subjected to the transformer operational efficiency. The transformer efficiency is defined as the ratio of the power output at the secondary winding to the power input at the primary winding. The efficiency of the transformer, η is shown in equation (1) as follows:

$$\eta = \frac{P_{out}}{P_{out} + P_{losses}} \times 100\% \quad (1)$$

where P_{out} is the power output of the secondary winding in kW and P_{losses} is the total transformer losses in kW.

Transformer losses can be categorised into no-load losses and load losses. No-load losses are the transformer losses when the transformer is operated without a load. The no-load losses are mainly contributed by hysteresis loss and eddy current loss (Borge-Diez *et al.*, 2013) and it is independent of the operating loads. Load losses occur when a load is connected to the transformer. Load losses are mainly contributed by the copper losses of primary and secondary windings in which the heat is dissipated via the impedance of the windings (Borge-Diez *et al.*, 2013). Copper losses are proportional to the square of the load current. Due to the different characteristics of the no-load losses and load losses, the transformer efficiency varies at different load levels. Based on equation (1), the transformer efficiency, η at different load level can be expressed by equation (2):

$$\eta = \frac{i \times S_{rated} \times pf}{i \times S_{rated} \times pf + P_{loss,nl} + i^2 \times P_{loss,fl}} \times 100\% \quad (2)$$

where i is the percentage of the load level of the transformer ranging from 0 to 1, S_{rated} is the power rating of the transformer in kVA, pf is the power factor, $P_{loss,nl}$ is the total no-load losses in kW, and $P_{loss,fl}$ is the maximum load loss in kW.

Based on equation (2), the load level that gives the maximum efficiency of a transformer is strongly dependent on the no-load losses and the maximum load losses. Maximum efficiency occurs at a load level when the load losses are equal to the no-load losses (Brosan and Bishop, 1960). Typically a power transformer is designed such that the maximum efficiency is achieved at a load level ranging from 40 to 50 % (Harden, 2011). From the transformer datasheet, the no-load losses and the load losses for the 132/33 kV BSS transformers are shown in Table 3.9.

Table 3.9 Losses on 132/33 kV BSS transformers

Transformer Ratings	50 MVA	40 MVA
No-load Losses at Rated Voltage (kW)	30	21
Load Losses at Rated Power (kW)	140	175

The load efficiency curve of the transformer shown in Figure 3.17 is plotted using equation (2). It can be seen that the maximum efficiency of the transformer occurs when it is operated at a 45 % load level. The power losses of the transformer at different load level and different power factor can be calculated using equation (3) as follows:

$$P_{loss} = P_{in} - P_{out} = \frac{S_{out} \times pf}{\eta} - S_{out} \times pf \quad (3)$$

where P_{in} is the active power input of the transformer in kW, P_{out} is the active power output of the transformer in kW, η is the efficiency of the transformer, S_{out} is the apparent power output of the transformer in kVA, and pf is the power factor.

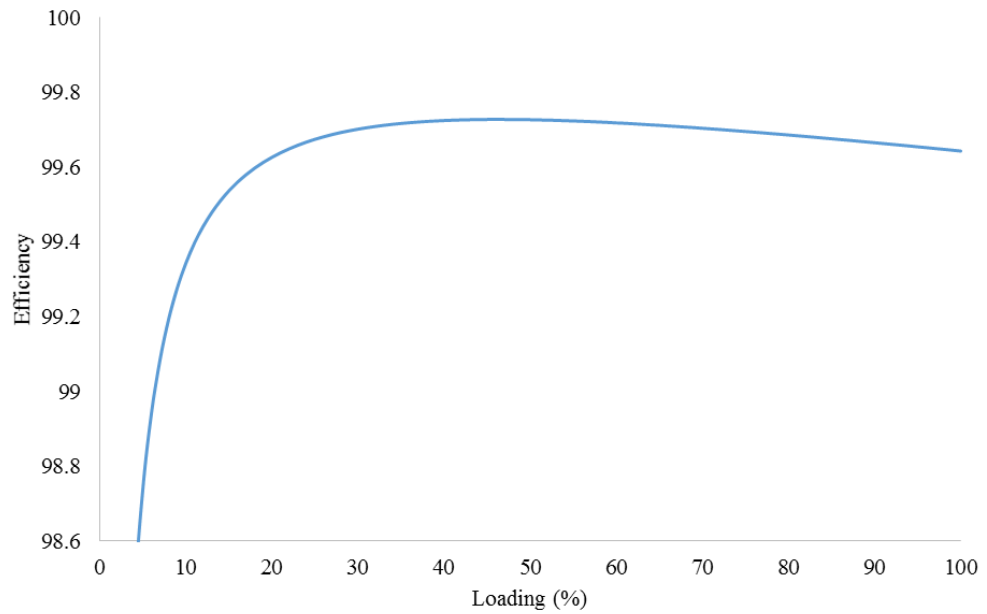


Figure 3.17 Efficiency curve for transformer rated 50 MVA at a power factor of 0.95

3.5 Dynamic Traction Load Modelling

In dynamic analyses, only the distribution network under Jinjang BSS is chosen for the investigation. This network consists of 8 TPSSs and 15 stations, starting from Damansara Damai station to Kampung Baru North station, with a total track length of 17.28 km. Figure 3.18 shows the route for the MRT2 line and the section under Jinjang BSS.

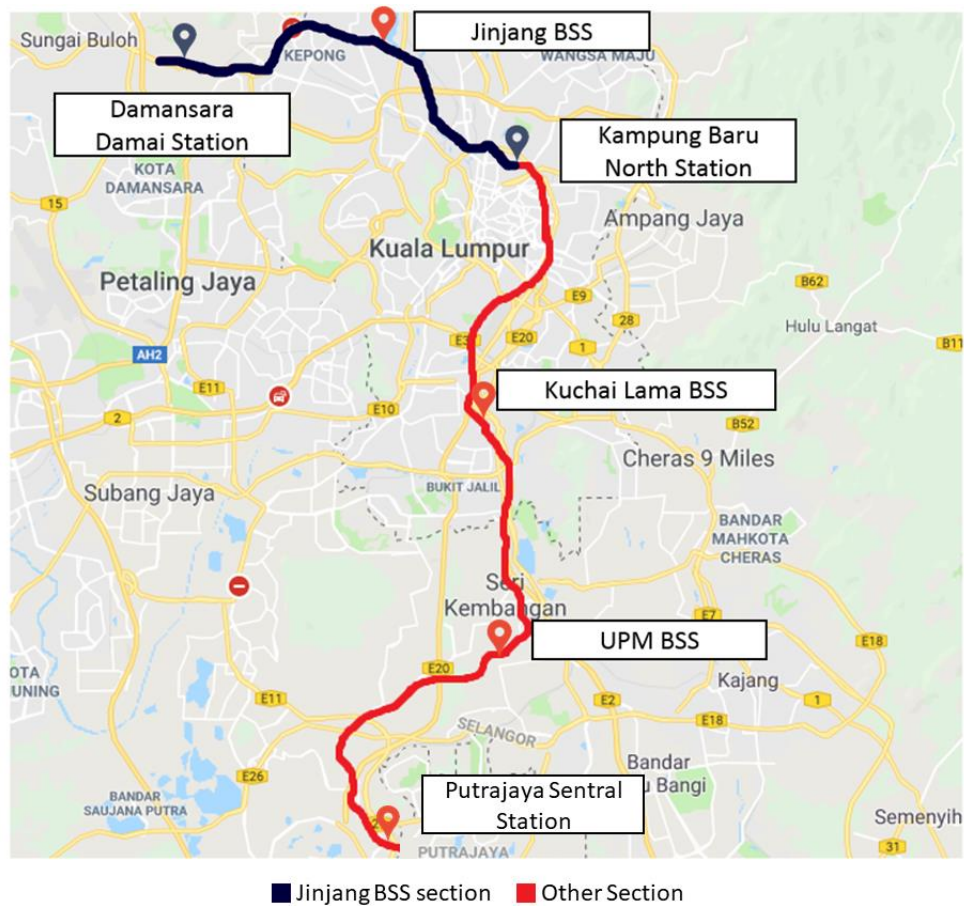


Figure 3.18 The Jinjang BSS section on the map

3.5.1 Low Voltage Traction Network

MRT2 adopts the standard 750 V DC third rail system. A conducting rail is placed on the sleeper ends outside of the running rail to supply power to the train through the contact shoes attached to the train. The material of the conducting rail is the Aluminium/Stainless Steel (ALSS) conductor, composed of 95 % of aluminium and 5 % of steel. The return current flows back to the TPSS through the running rail which is made of carbon steel. The resistances of the conducting rail and the running rail are 7 mΩ/km and 22 mΩ/km, respectively, as provided

by the manufacturer. Figure 3.19 shows the position of the conducting rail of a third rail system on top of the running rails.

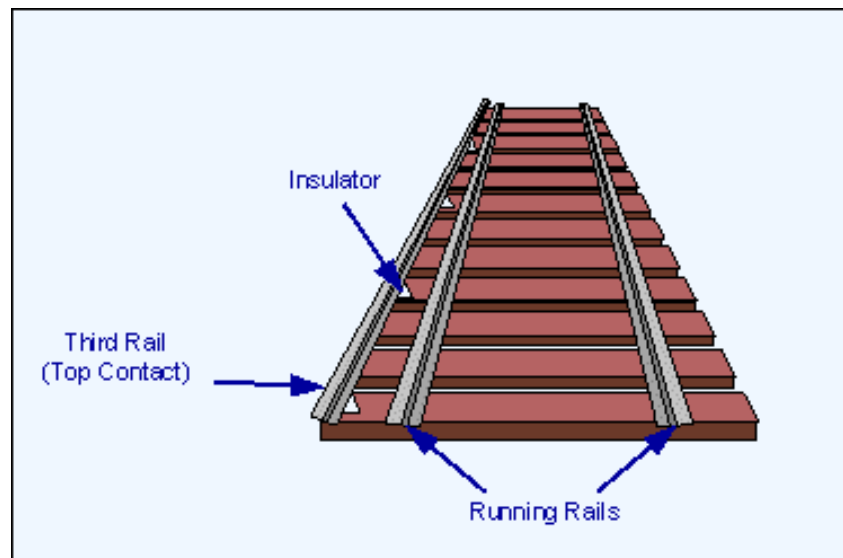


Figure 3.19 Structure of tracks of the third rail system

Figure 3.20 shows the schematic diagram of the low voltage traction network. It is shown that the DC track sections are fed by the TPSS from each of the end. Such configuration allows train services to be maintained in case of maintenance or failure of any TPSS. Each DC track section has a length of between 1 km to 3 km to ensure that the peak accelerating current can be taken by the trains at any location while maintaining the rail voltage above the minimum required level.

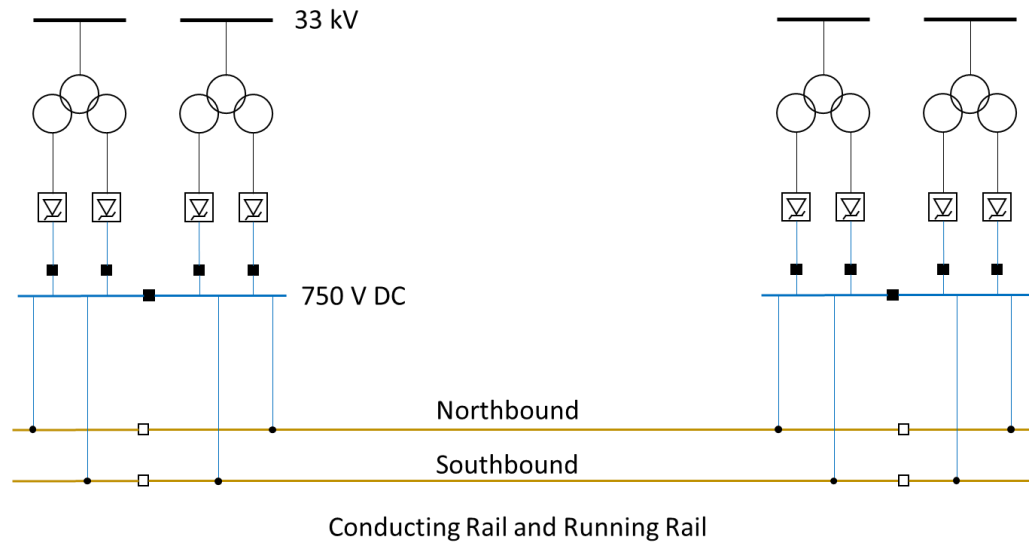


Figure 3.20 Schematic diagram of the low voltage traction network

3.5.2 Rolling Stock

The term ‘rolling stock’ is often used in the industry to refer to the vehicle. The parameters of the rolling stock are provided by the manufacturer (Colas Rail System Engineering Sdn. Bhd., 2018), and is shown in Table 3.10.

Table 3.10 Parameters of the rolling stock for MRT2

General	
Train Configuration	4 Cars (M-T-T-M) M = Motor Car T = Trailer Car
Length x Width x Height	90 m x 2.984 m x 3.7 m
Frontal Area, A_F	11.04 m ² (Width x Height)
Number of Axles	4 per car
Total Train Weight (AW3P)	218 ton
Total Weight of Motor Car, W_m	124.48 ton
Total Weight of Trailer Car, W_t	105.25 ton
General Dynamic Performance	
Maximum Operating Speed	110 km/h
Maximum Acceleration Rate	1.0 m/s ²
Service Braking Rate	1.1 m/s ²
Maximum Voltage	900 V
Minimum Voltage	500 V
Traction Motor Efficiency	90 %
Auxiliaries	
Auxiliary Voltage	750 V
Auxiliary Power	236.48 kVA

The vehicle model for MRT2 is developed using Train Rolling Stock Library in ETAP. Train Rolling Stock Library provides a table to insert the parameters of

the rolling stock, including the weight, dimensions, Davis coefficients, auxiliary power, etc., as shown in Figure 3.21. On the second tab of the library, the tractive effort curve and braking effort curve of the rolling stock can be imported as point-data, as shown in Figure 3.22.

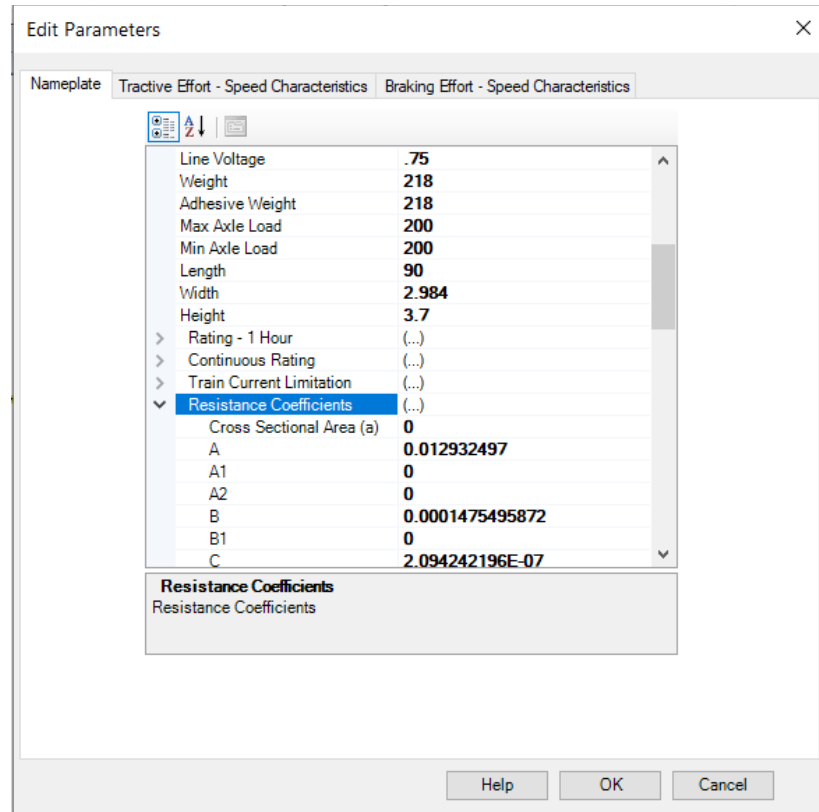


Figure 3.21 Train Rolling Stock library in ETAP

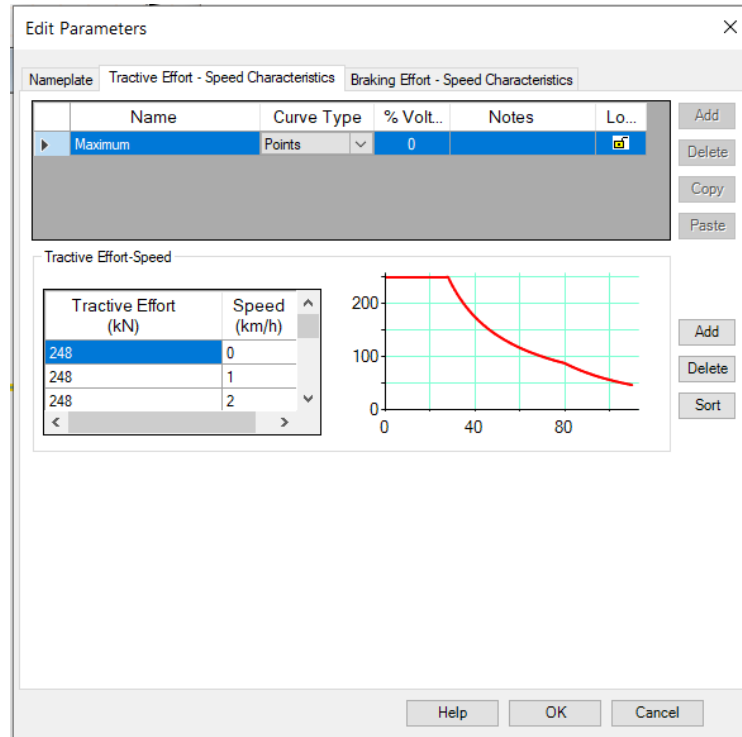


Figure 3.22 Tractive effort curve in Train Rolling Stock Library

3.5.3 Train Dynamics

The motion of the train can be expressed by standard Newtonian equations of motion. The train dynamics in the longitudinal direction is governed by the tractive effort, the gradient of the track, and the train resistance, as shown in equation (4).

$$M_{eff}a = TE - F_{rr} - F_g \quad (4)$$

where M_{eff} is the effective mass of the train, a is the net acceleration of the train, TE is the tractive effort (or braking effort when train decelerates) in kN, F_{rr} is the rolling resistance in kN expressed in the form of Davis equation and F_g is the track gradient resistance in kN.

3.5.3.1 Train Effective Mass

During the acceleration of a train, the rotating parts of the train are also accelerated in a rotational sense. To compensate for the rotational effect of the train motor and wheels, the effective mass of the train should be increased. Hence the effect of rotational inertia on the effective mass can be expressed by equation (5). In ETAP, a constant with a value of 8 is used by the software to adjust the effective mass.

$$M_{eff} = m \left(1 + \frac{\xi}{100} \right) \quad (5)$$

where m is the initial mass of the train and ξ is a constant used by the software to adjust the effective mass.

In this study, the weight of the train is assumed to be constant. The weight of the train is based on AW3P condition, which refers to the simulation of a train with a crush load, in other words, the maximum number of passengers that can be riding in the vehicle, including those who are standing and sitting. The number of passengers is assumed to be constant throughout the trip in this study.

3.5.3.2 Rolling Resistance

When a train is moving, there are friction and aerodynamic drag acting in the opposite direction. The summation of these forces is the train rolling resistance and is dependent on the train weight, speed, and shape. The rolling resistance

can be expressed in the form of the Davis Equation, as shown in equation (6). In this study, the Davis coefficients A, B, and C are provided by the rolling stock manufacturer.

$$F_{rr} = A + BV + CV^2 \quad (6)$$

where V is the speed of the train in km/h, A is Davis Equation constant in kN, B is Davis Equation linear term constant in N/(km/h), and C is Davis Equation quadratic term constant in $/(km/h)^2$.

The formula for rolling resistance in the unit of kN is given by the manufacturer (Colas Rail System Engineering Sdn. Bhd., 2018a), as expressed by equation (7).

$$F_{rr} = (1.65 + 0.024V)W_m + (0.78 + 0.0028V)W_t + [(0.028 + 0.078(n - 1)]A_F V^2 \quad (7)$$

where V is the speed of the train in km/h W_m is the total weight of motor car including rotating inertia in ton, W_t is the total weight of trailer car including rotating inertia in ton, n is the number of cars, and A_F is the frontal area of the train in m^2 .

By rearranging equation (7) into the form of equation (6), the rolling resistance can be expressed as equation (8).

$$F_{rr} = 2.819283962 + 0.032165831V + (4.565447 \times 10^{-5})V^2 \quad (8)$$

Both equation (7) and equation (8) have included the train weight into consideration. the value of the coefficients from equation (8) must be changed if there is a change in the weight of the train. To normalise the equation, it is required to input the value of the Davis coefficients in per ton values. Hence, by dividing the total train weight, the formula of rolling resistance can be expressed as equation (9). The final value of Davis coefficients to be input into ETAP software is as listed in Table 3.11.

$$F_{rr} = 0.012932497 + 0.0001475495872V + (2.094242196 \times 10^{-7})V^2 \text{ kN/ton} \quad (9)$$

Table 3.11 Davis coefficient of MRT2 train used in ETAP software

Davis Coefficients	Values
A	0.012932497
B	0.0001475495872
C	$2.094242196 \times 10^{-7}$

3.5.3.3 Gradient Resistance

The train is affected by the gravitational force when it is moving uphill or downhill. The magnitude of the gravitational force depends on the gradient of the track, which is expressed by equation (10).

$$F_g = mg \sin\left(\tan^{-1}\frac{G}{100}\right) \quad (10)$$

where g is the standard gravity of Earth in constant of 9.81 and G is the track gradient in percentage.

3.5.3.4 Curve Resistance

The effect of the curvature resistance is negligible when the train is running at a speed of less than 200 km/h (Tian, 2017). The maximum operating speed of the rolling stock in MRT2 is 110 km/h. Hence, to simplify the model, track curvatures are not considered in the track modelling.

3.5.3.5 Tractive Effort and Braking Effort

Traction motors produce tractive effort to overcome the rolling resistances and gradient resistance. The maximum value of tractive effort at every speed is determined by the tractive effort curve of the rolling stock. The curves also determine the maximum acceleration and deceleration of the train if it is below the pre-defined limit. A typical tractive effort curve for a traction motor has three distinct phases. At low speed, the traction motor operates in the constant torque region, whereby the tractive effort is maintained as the speed increase. In this region, the motor power consumption increases as the speed increases. As the speed increases beyond v_1 , the traction motor falls into the constant power region. While the power remains constant, the tractive effort decreases at a rate of $1/v$. At higher speed beyond v_2 , the traction motor operates at a reduced

power region. In this region, the tractive effort reduces at a rate of $1/v^2$, while the power decreases from the maximum value. Figure 3.23 shows the tractive effort curve of the MRT2 rolling stock, provided by the manufacturer.

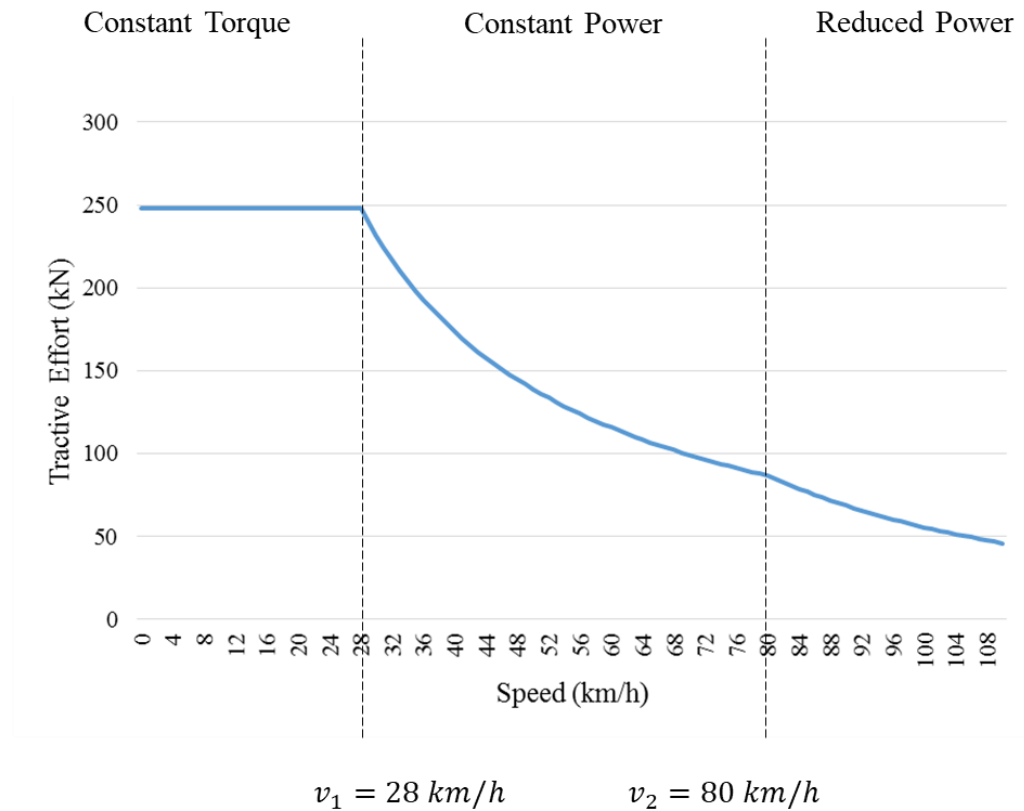


Figure 3.23 Tractive effort curve

Similar to the tractive effort, the traction motor produces a braking effort to decelerate the train during braking. The maximum value of braking effort at every speed is determined by the tractive effort curve of the rolling stock. Figure 3.24 shows the braking effort curve of the MRT2 rolling stock, provided by the manufacturer (Colas Rail System Engineering Sdn. Bhd., 2018a).

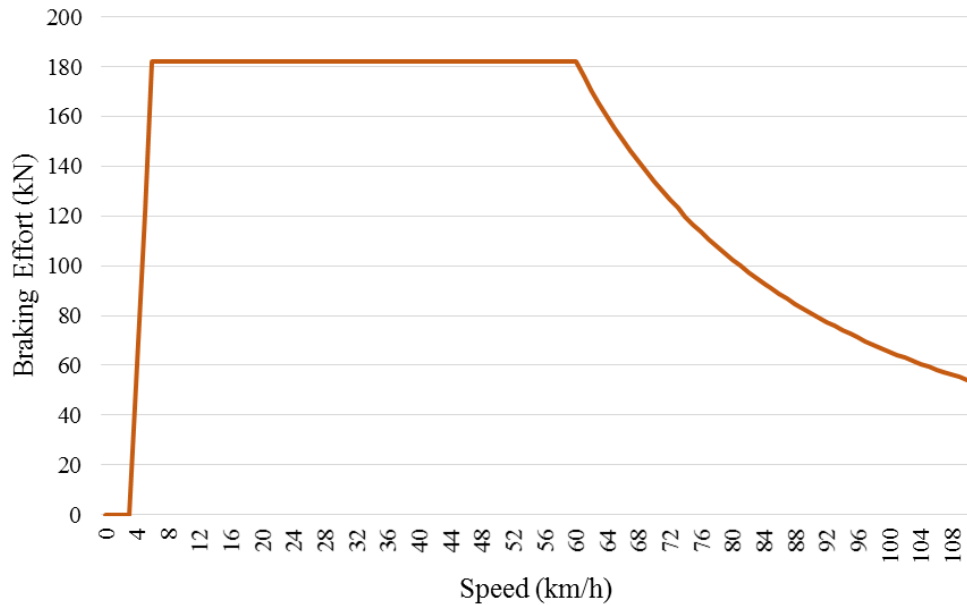


Figure 3.24 Braking effort curve

3.5.3.6 Train Power Consumption

The total power demand of a train is the summation of traction motor power and train auxiliary power. Traction motor power can be calculated from the tractive effort produced by the traction motor and the speed of the train. The auxiliary power includes the air conditioning, lightings, door operation, etc., and is defined as a constant value throughout the journey. Hence, the electrical power demand of a train in kW is expressed by equation (11). As regenerative braking is not considered in this study, therefore no power is generated by the traction motor during the train braking stage. Hence, the power consumption of the train during the braking stage is expressed by equation (12).

$$P = \frac{TE \times v}{\eta} + P_{aux} \quad (11)$$

$$P = P_{aux} \quad (12)$$

where TE is the tractive effort in kN, v is the train traveling speed in m/s, η is the efficiency of the train motor with a value of 0.9 provided by the manufacturer, and P_{aux} is the auxiliary power with a value of 236.48 kW.

3.5.4 Track Modelling

The track modelling of the MRT2 is done on the Geospatial Diagram of the ETAP. Unlike the schematic diagrams in One-line View where the lines and symbols are just graphical representations of the electrical network, railway tracks modelled in the Geospatial Diagram are accurate representation of size, length, and dimension in real life. As track curvatures are not considered in this study, therefore the railway tracks in Geospatial Diagram appear as a straight line, different from what we can see in real life. Figure 3.25 shows the straight railway track (yellow and blue lines), railway stations (blue square), and markers for speed limits and elevations (tiny circles on the track) in Geospatial Diagram.

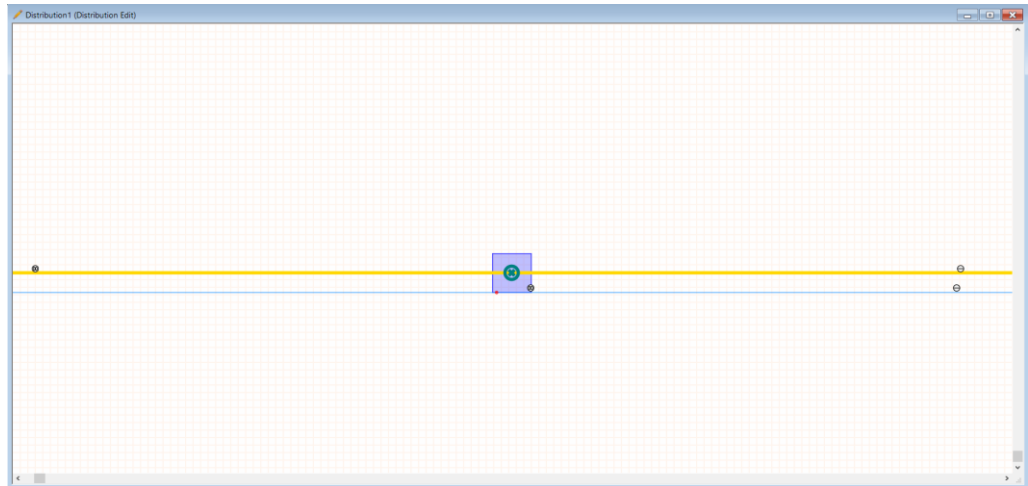


Figure 3.25 Track models in Geospatial Diagram

The track gradients and railway station elevations are marked by the Elevation Markers in Geospatial Diagram. Figure 3.26 shows the Elevation Marker Editor in ETAP, whereby the elevation of the track at this position is labelled by parameter ‘Z’ in a unit of meter. Equation (13) shows the formula to convert the track elevation in meter to track gradient in percentage. Figure 3.27 shows the elevation of the track along the line.

$$G = \frac{Z_{i+1} - Z_i}{D_{i+1} - D_i} \times 100\% \quad (13)$$

where Z is the track elevation in m, and D is the location of the Elevation Markers in m.

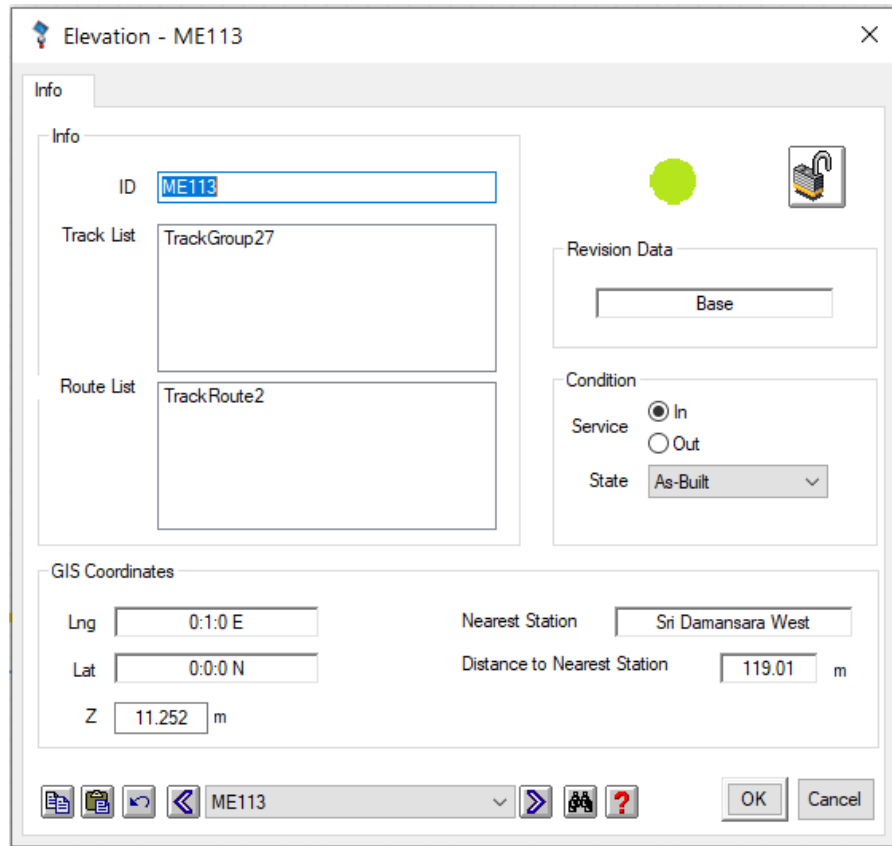


Figure 3.26 Elevation Marker Editor in ETAP

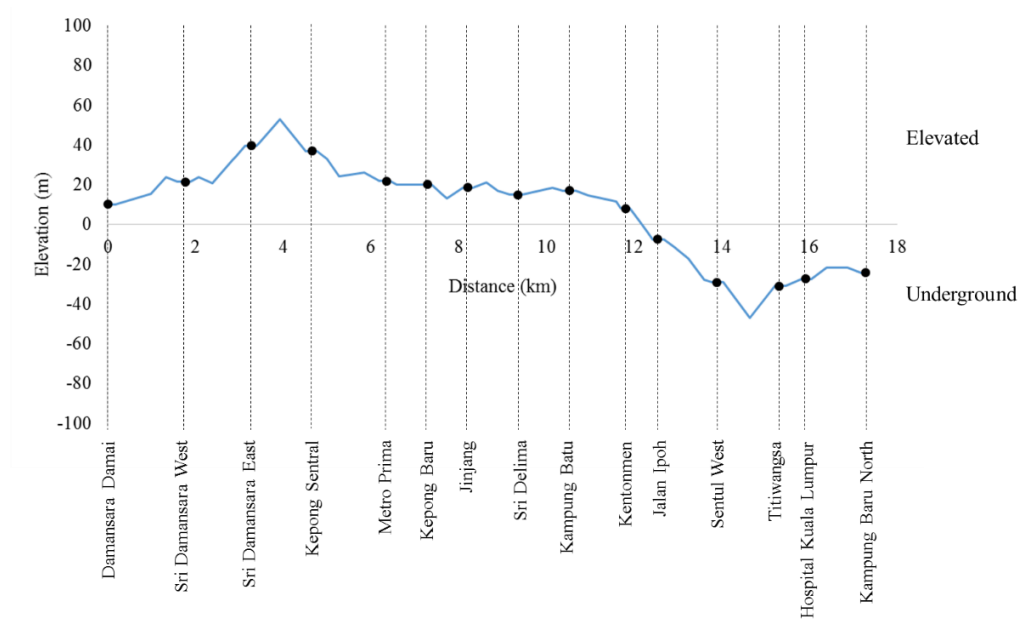


Figure 3.27 Stations and track elevations

By using Speed Limit Markers, the train speed limits between 70 km/h to 110 km/h are defined along the track. Figure 3.28 shows the Speed Limit Marker in ETAP. There is no freight train in this study, therefore the speed limits for the freight train are ignored. Figure 3.29 shows the speed limits along the track for both the directions the trains travel.

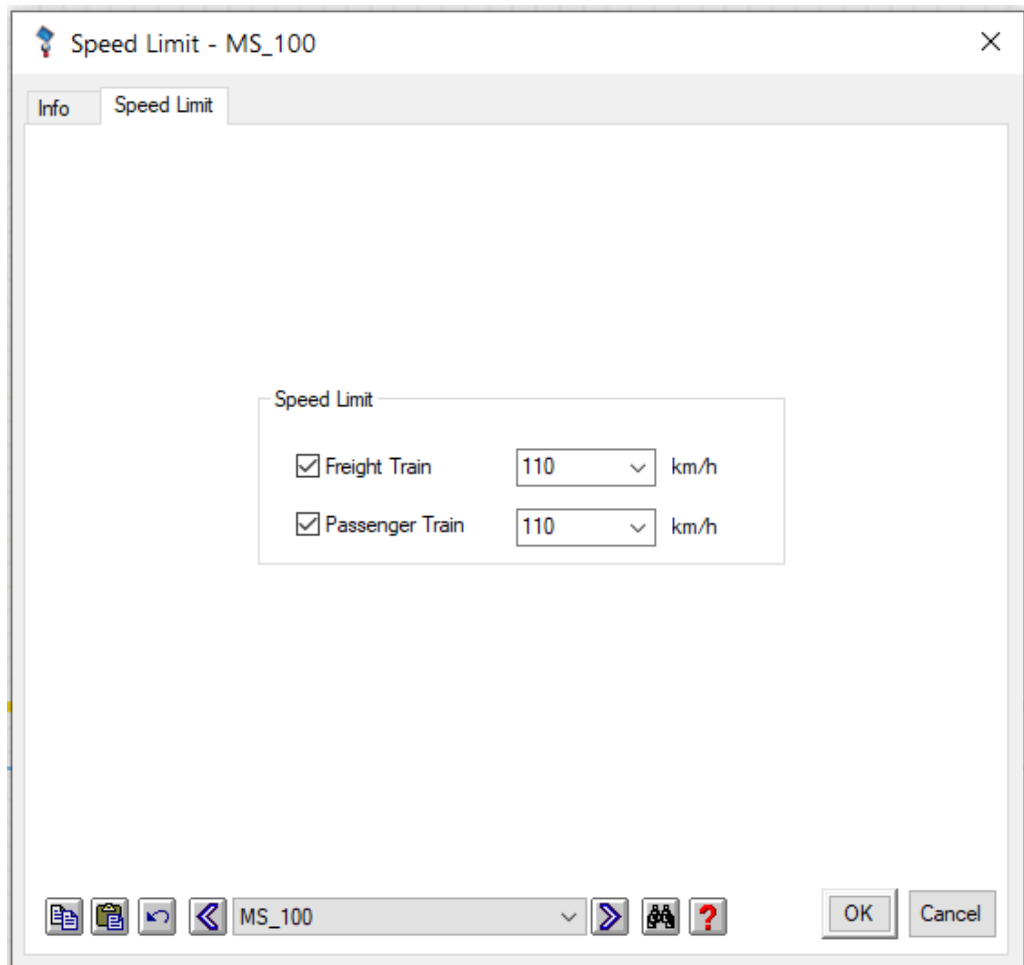
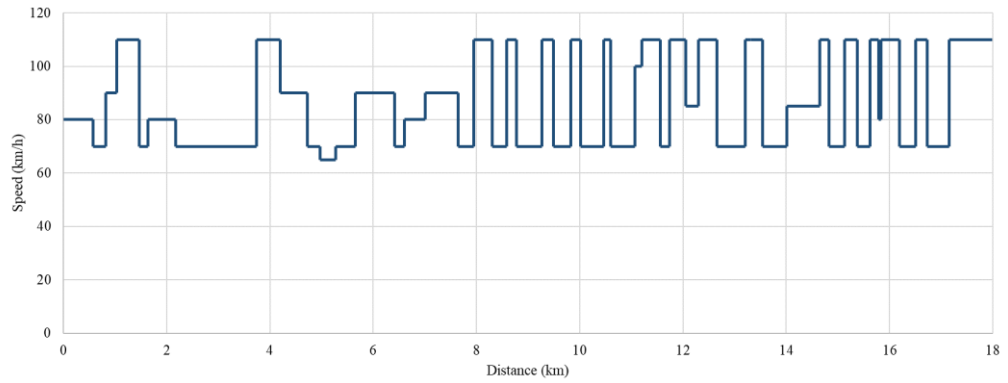
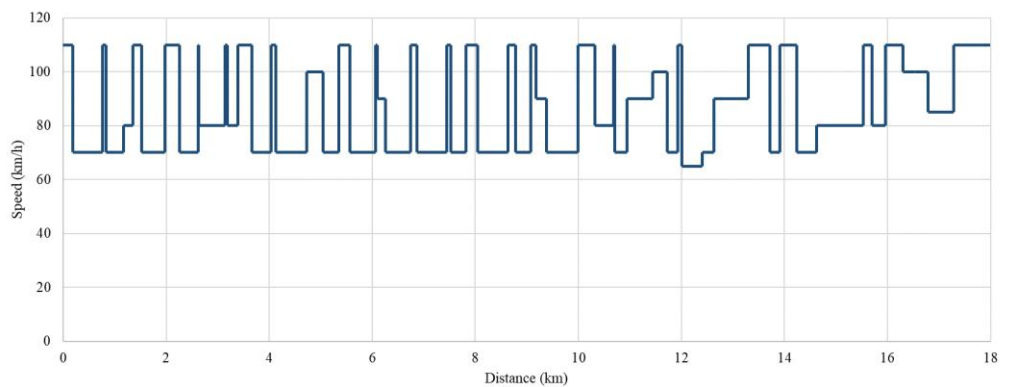


Figure 3.28 Speed Limit Marker Editor in ETAP



(a)



(b)

Figure 3.29 Speed limit along the line for (a) northbound (b) southbound

3.5.5 Train Schedules and Headway Intervals

Headway is defined as the average time interval between consecutive trains and is often used to describe the railway traffic density. A larger headway indicates a longer time interval between the departure time of trains, which leads to a lower power demand and energy consumption of the railway distribution system. Based on previous MRT projects in Malaysia, the railway system is operated at 3 minutes and 6 minutes headway intervals at peak period and off-peak period, respectively. However, during the design stage, it is desired to simulate the

headway interval from 2 minutes to 7 minutes. Therefore, this study has included the headway interval from 2 minutes to 7 minutes to investigate how the headway interval affects the energy consumption, power demand, and power losses of the transformers.

ETAP-Etrax software provides two schedule modes for the simulations, namely free schedule mode and fixed schedule mode. In free schedule mode, the trains are traveling at maximum speed and shortest traveling time. At the end of the simulation, the system will update the train arrival and departure times. In contrast, the fixed schedule mode allows the users to provide accurate train arrival and departure times to the system, and the train will accelerate or brake accordingly.

The free schedule mode is used in this study for simulations. The acceleration limit and deceleration limit are set to 1 ms^{-2} and -1.1 ms^{-2} , respectively. The train dwell time at each station is set to 30 seconds. Based on these limitations and track parameters, the speed profile of the trains was obtained.

The timetables are configured in the Train Schedule tab of the Etrax Editor, as shown in Figure 3.30. For free schedule mode, only headway interval, train departure time at the first station, and station dwell time are required. The train arrival times and train departure times at all the stations are remained blank before the simulation and will be updated after the simulation, as discussed in Chapter 4.

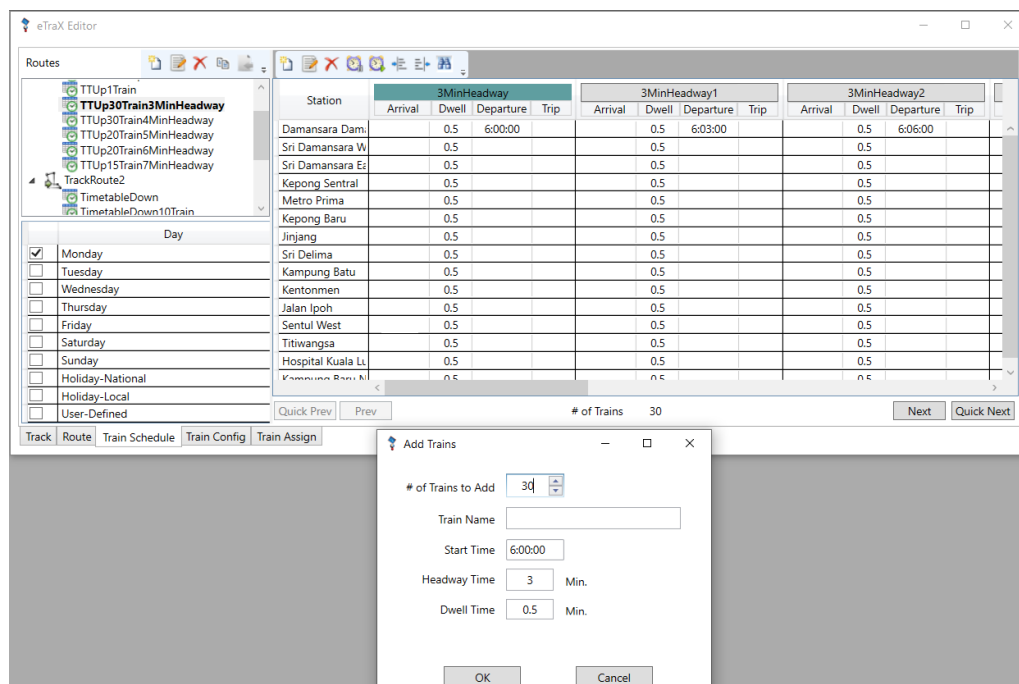


Figure 3.30 Configure train timetables in Etrax Editor

3.5.6 Load Flow Solver

In ETAP-Etrax simulation, train dynamics have been considered in the dynamic load flow analyses of the MRT2 power supply and distribution systems. The power consumption of the trains on track is first calculated from the input parameters such as track gradient, timetable, locomotive tractive and braking effort curves, Davis coefficients for rolling resistance, train speed limit, and the train acceleration and deceleration limit defined by the railway operators. The calculated train power demand is then attached to the high voltage traction power supply and distribution network. The software then performs iterative Newton-Raphson 3-phase power flow calculations using the current injection method to solve the bus voltages, branch power factors, currents, and power flows of the electrical network on a time-domain series. These procedures are repeated for all

time steps until all the trains on the track have completed their trip. The calculation method implemented by ETAP-Etrax software is summarised in Figure 3.31.

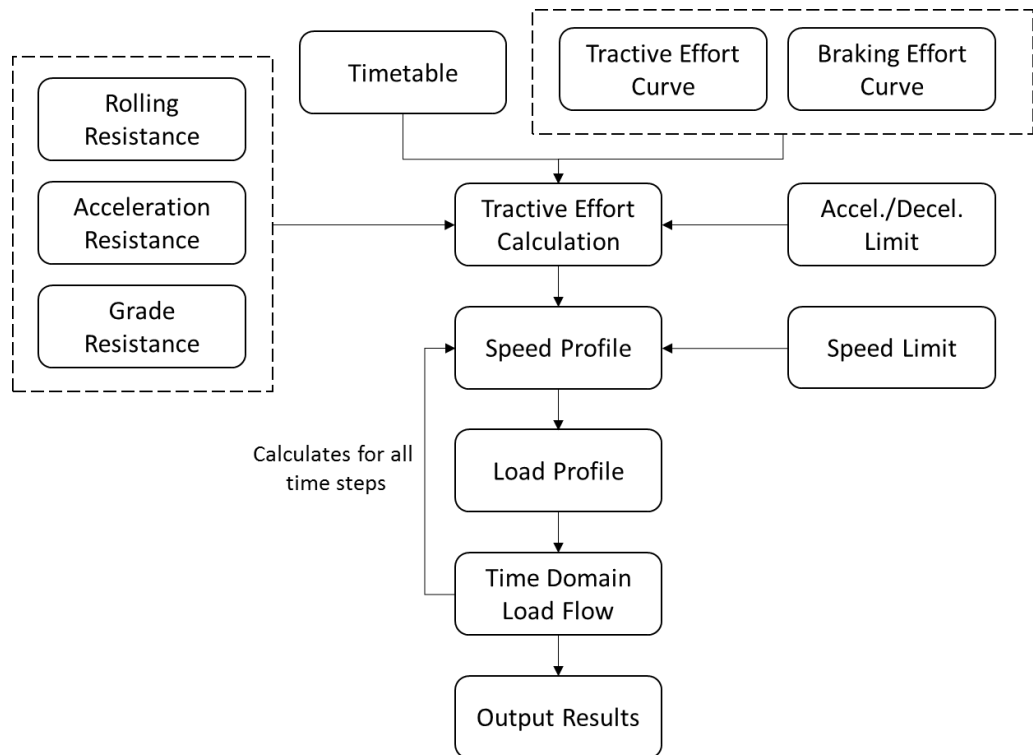


Figure 3.31 Load flow calculation with train dynamics

To simplify the study, the following assumptions have been made for the simulation model:

1. The weight of the trains is assumed to be constant throughout the journey.
2. Simplified timetables are used, whereby all trains in the same direction share the same timetable. The trains are assigned with the same station dwell time and interstation trip time. The train dwell time

for all the stations is constant at 30 seconds. No time shift between train departures of both directions is considered.

3. The impacts of regenerative braking on the system are not considered in this study. Due to the use of simplified timetables, most of the time the regenerated energy from braking trains is not utilised by the other trains for acceleration. Bidirectional power flow for DC traction substations is not considered in this study due to its sophisticated operating strategy of the inverters and rectifiers in preventing circulating current.

However, the impacts of regenerative braking on the traction power supply systems will be investigated in future works, whereby a simulation model with bidirectional DC traction substations and the control strategies of inverters will be developed. Furthermore, other parameters such as time-shift between train departures of both directions and the dwell time “noise”, will also be included in future works.

3.6 Short-circuit Analyses

The short-circuit current of the system does not have any impact in finding the optimal transformer operation mode. However, it is crucial for power system protection. As mentioned in Chapter 2, parallel transformer operation results in increase of short-circuit current. Hence, short-circuit analyses have to be done to

ensure that the power supply system can withstand the short-circuit current. This section presents the procedures to perform the short-circuit analysis in accordance with IEC 60909 standard. For IEC 60909, the analysis takes into account the contribution of generating units and motors to the short-circuit level ('IEC 60909–0:2016: Short-circuit currents in three-phase a.c. systems - part 0: Calculation of currents', 2016). In the calculation, the fault location is replaced with an equivalent voltage source. The voltage source value is then adjusted by multiplying a voltage factor 'c' corresponding to the nominal voltage, as shown in Table 3.12.

Table 3.12 Voltage factor 'c' as per IEC 60909

Nominal Voltage, U_n	Voltage Factor, c
< 1 kV	1.05
> 1 kV	1.10

The initial symmetrical short-circuit current (I''_k) can then be calculated using equation (14).

$$I''_k = \frac{cU_n}{\sqrt{3}Z_k} \quad (14)$$

where U_n is the nominal voltage in V, c is the voltage factor as per IEC 60909, and Z_k is the equivalent sub-transient impedance at the fault location.

Short-circuit analysis in ETAP is based on IEC 60909 by default. The voltage factor 'c' can be configured in Short-circuit Study Case Editor in ETAP, as

shown in Figure 3.32. In this study, only the maximum short-circuit current simulation is done. Based on transformers parameter from Table 3.2, Table 3.5, and Table 3.8, the negative impedance tolerance values are considered for the short-circuit analysis.

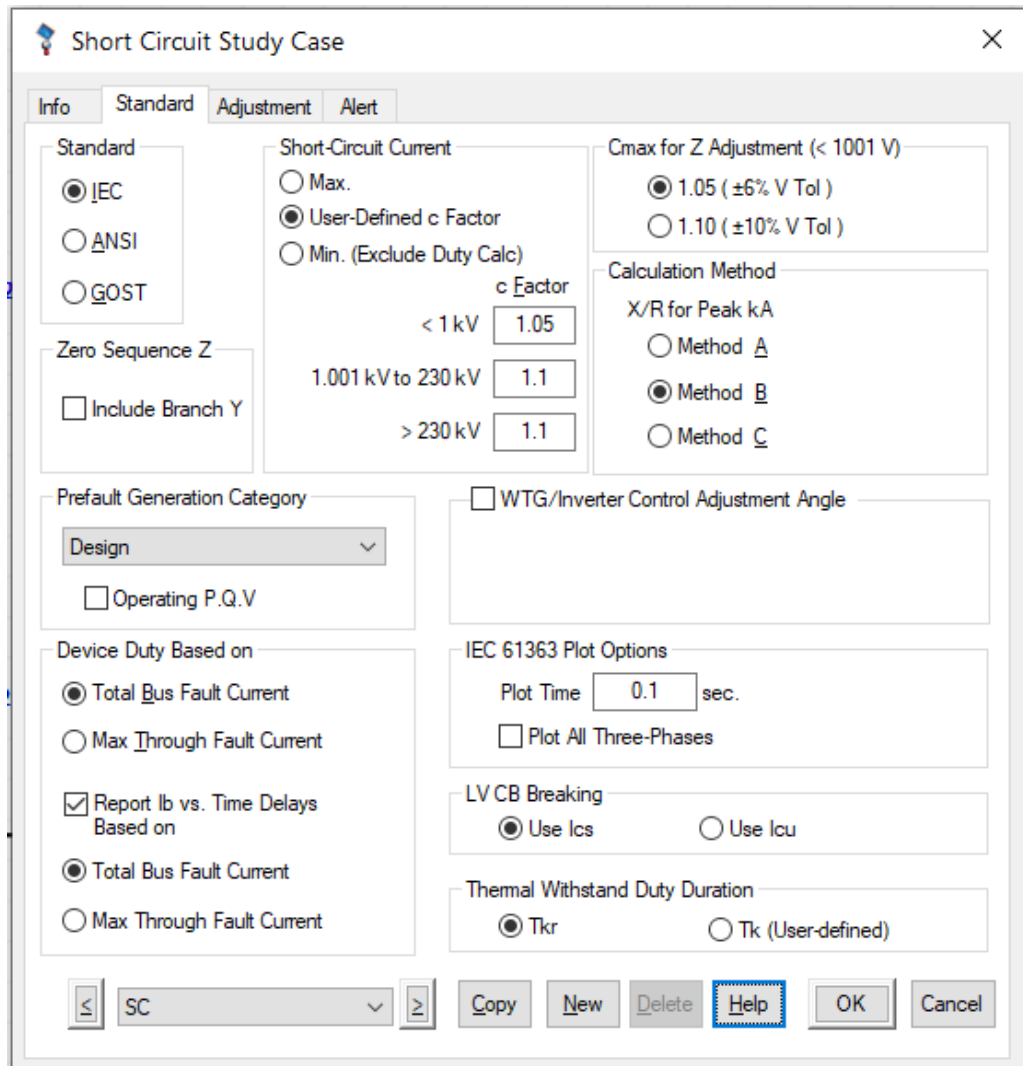


Figure 3.32 Short-circuit Study Case Editor in ETAP

The utility grids at different locations contribute to different values of maximum short-circuit current by generating units. Table 3.13 shows the X/R ratio and the short-circuit contribution by the grid at different locations. According to the

Malaysian Distribution Code, the maximum short-circuit currents must be lower than 90 % of the short-circuit breaking withstand capability of the protective devices and the make capacity of the switchgear (Malaysian Energy Commission, 2017). Table 3.14 lists down the short-circuit ratings of both the 132 kV and 33 kV switchgear, and the acceptable limit of the short-circuit current.

Table 3.13 Short-circuit current contribution and X/R ratio by the grid

Locations	Maximum Fault Level (kA) ^a	X/R Ratio ^a
Jinjang BSS	14.5	20
Kuchai Lama BSS	15	20
UPM BSS	23.7	20

Footnotes:

a- Data collected from (Colas Rail System Engineering Sdn. Bhd., 2018b)

Table 3.14 Rated short-time withstand current for different switchgear

Switchgear	Rated Short-time Withstand Current ^a	Acceptable Limit
132 kV	31.5 kA for 3s	28.35 kA
33 kV	25 kA for 3s	22.5 kA

Footnotes:

a- Data collected from (Colas Rail System Engineering Sdn. Bhd., 2018b)

CHAPTER 4

RESULTS AND DISCUSSIONS

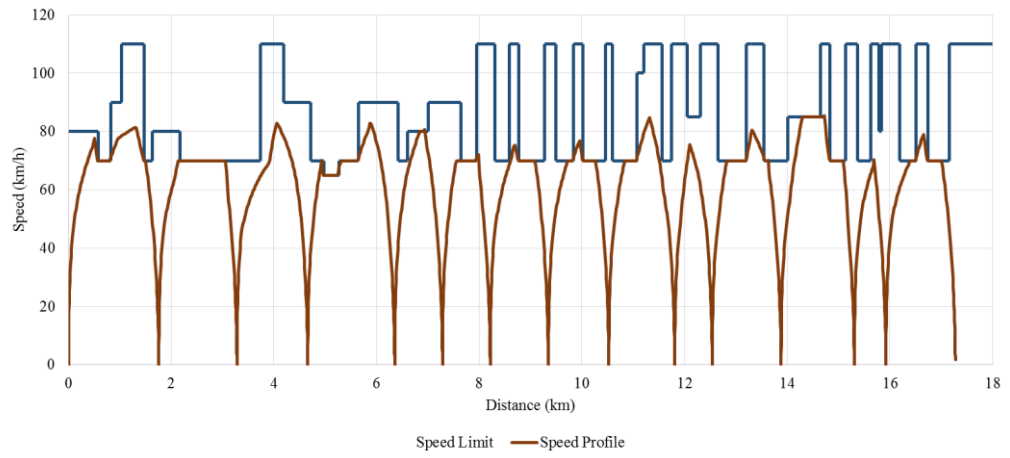
4.1 Introduction

This chapter discusses the results of the dynamic analyses at the low voltage traction network. The performance of the BSS transformers based on the train dynamics is investigated. The BSS transformer losses at different scenarios and different headway intervals of train schedules are studied. At the end of the chapter, the results of the short-circuit analysis are analysed to investigate the fault level for both the parallel mode and non-parallel mode.

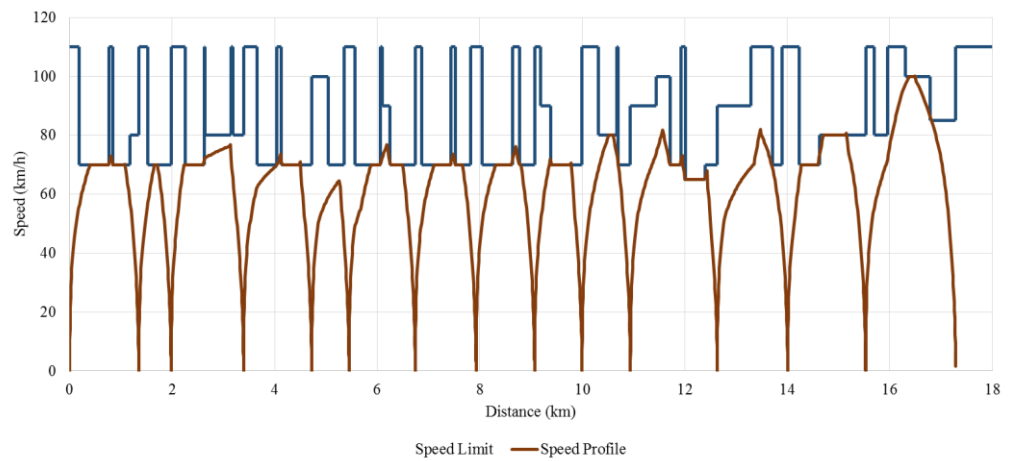
4.2 Train Dynamic Profiles

Based on the parameters of the rolling stock and tracks in the previous chapter, the single train speed profiles for both directions are as shown in Figure 4.1. The speed profile is plotted in the spatial domain to visualise the speed limit of the track. As shown in the figure, the speed of the train is restricted by the speed limit along the track during the simulation. From the speed profiles, the change of the train speed during acceleration, cruising, and braking can be observed. It can be seen that the vehicle accelerates and decelerates in curve lines, indicating that the traction motor operates at both the constant torque region and constant power region. As the speed profiles are speed-distance graphs, the events of the

vehicle stopping at the stations can be observed, which is when speed equals 0, but the train dwell time at the stations cannot be derived from the speed profiles.



(a)

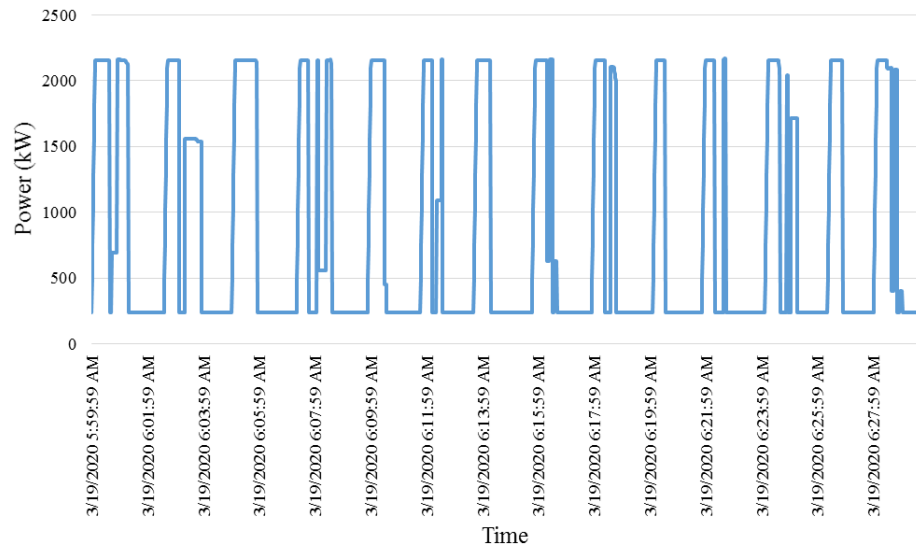


(b)

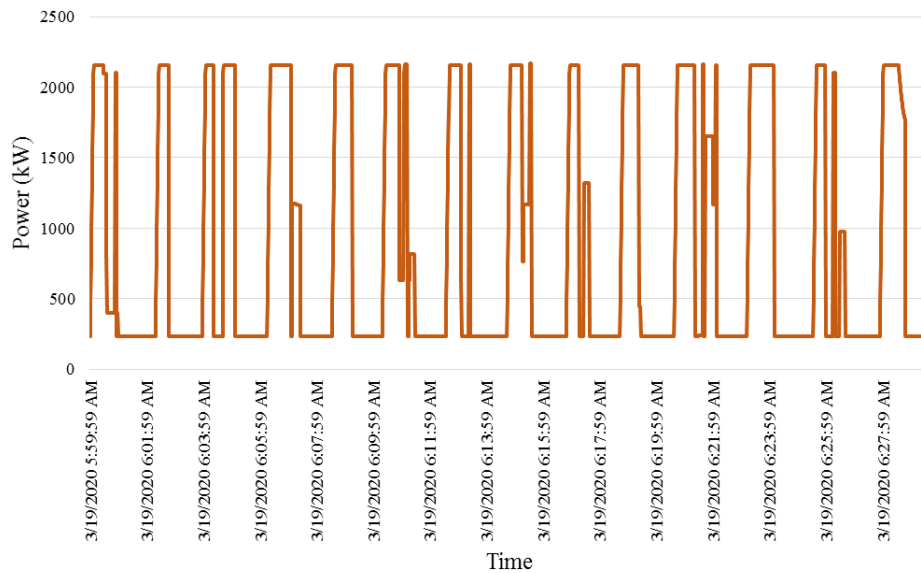
Figure 4.1 Single train speed profile for (a) northbound (b) southbound

Figure 4.2 shows the power profiles of a train in both directions throughout the whole trip. The power demand of the train is the summation of the auxiliary power and traction power. During the acceleration phase of the train, the

instantaneous power demand reaches the maximum of 2153 kW. As regenerative braking is not considered in this study, thus during the braking phase, the power consumption of the train is 236.48 kW, which is the auxiliary power.



(a)



(b)

Figure 4.2 Single train power profile for (a) northbound (b) southbound

Table 4.1 and Table 4.2 show the train arrival and departure time at each station for the northbound and southbound directions, respectively. The total trip times for the northbound and southbound are 28 minutes 21 seconds and 28 minutes 25 seconds, respectively. These train schedules are obtained based on free-schedule mode calculation. In other words, the total trip times obtained are the shortest possible trip time achievable by the vehicles.

Table 4.1 Train arrival and departure time for northbound

Station Names	Arrival	Dwell (s)	Departure	Trip (s)
Damansara Damai	05:59:30	30	06:00:00	114
Sri Damansara West	06:01:54	30	06:02:24	106
Sri Damansara East	06:04:10	30	06:04:40	99
Kepong Sentral	06:06:19	30	06:06:49	113
Metro Prima	06:08:42	30	06:09:12	73
Kepong Baru	06:10:25	30	06:10:55	74
Jinjang	06:12:09	30	06:12:39	85
Sri Delima	06:14:04	30	06:14:34	87
Kampung Batu	06:16:01	30	06:16:31	92
Kentonmen	06:18:03	30	06:18:33	65
Jalan Ipoh	06:19:38	30	06:20:08	95
Sentul West	06:21:43	30	06:22:13	93
Titiwangsa	06:23:46	30	06:24:16	59
Hospital Kuala Lumpur	06:25:15	30	06:25:45	96
Kampung Baru North	06:27:21	30	06:27:51	0

Table 4.2 Train arrival and departure time for southbound

Station Names	Arrival	Dwell (s)	Departure	Trip (s)
Kampung Baru North	05:59:30	30	06:00:00	97
Hospital Kuala Lumpur	06:01:37	30	06:02:07	59
Titiwangsa	06:03:06	30	06:03:36	98
Sentul West	06:05:14	30	06:05:44	97
Jalan Ipoh	06:07:21	30	06:07:51	67
Kentonmen	06:08:58	30	06:09:28	94
Kampung Batu	06:11:02	30	06:11:32	88
Sri Delima	06:13:00	30	06:13:30	86
Jinjang	06:14:56	30	06:15:26	74
Kepong Baru	06:16:40	30	06:17:10	74
Metro Prima	06:18:24	30	06:18:54	112
Kepong Sentral	06:20:46	30	06:21:16	100
Sri Damansara East	06:22:56	30	06:23:26	102
Sri Damansara West	06:25:08	30	06:25:38	107
Damansara Damai	06:27:25	30	06:27:55	0

4.3 BSS Transformer Loadings and Losses

In real life, there are multiple trains running together on the tracks. The combination of the time-varying power demand of all the trains results in dynamic BSS transformer demand profiles. Figure 4.3 compares the demand profile of the BSS transformers between non-parallel mode and parallel mode. The demand profiles are the simulation results with 30 train trips in each direction, with a schedule of 2 minutes headway interval. For every simulated scenario, all the trains start at the first station of the respective tracks. With each train trip adding into the track one by one in 2 minutes interval, the maximum number of trains on the track occurs at the peak period from 6.28 am to 6.58 am. In real life, this peak period persists for a much longer time than the simulation

of only 30 trains. Therefore, the following analyses in the rest of this section refer only to the peak periods.

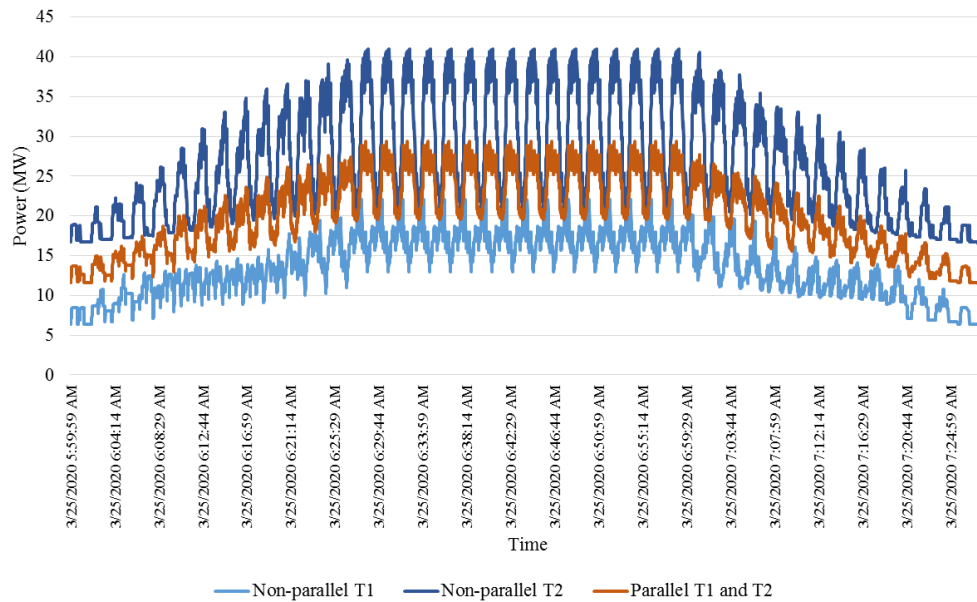


Figure 4.3 BSS transformer demand profile for non-parallel mode and parallel mode

It can be seen from Figure 4.3 that in parallel mode, both the BSS transformers have the same demand profile, indicating that the loads are equally distributed by both the transformers. On the other hand, in non-parallel mode, transformer T2 has a higher loading than transformer T1, due to the unequal distribution of station loads and traction loads during the design stage.

From the demand profiles as shown in Figure 4.3, the peak and average loading of the BSS transformers for both parallel and non-parallel modes are tabulated

in Table 4.3. It can be seen that the loads are not equally distributed among the BSS transformers for the non-parallel mode, with a discrepancy of 29.3 % for average loading between both the BSS transformers. Both the peak and average transformer loadings in non-parallel mode are not within the optimal efficiency range. Unequal load distribution among the BSS transformers results in transformers operating at different efficiency levels. On the other hand, the parallel mode results in average transformer loadings with the optimum range of transformer efficiency between 40 % and 50 %.

Table 4.3 Peak and average loading of the BSS transformers in parallel and non-parallel modes

Transformer (50 MVA)	Non-parallel			Parallel		
	Peak (MW)	Average (MW)	Average (%)	Peak (MW)	Average (MW)	Average (%)
T1	22.04	17.14	34.3	29.30	24.51	49.0
T2	41.00	31.85	63.6	29.30	24.51	49.0

On the other hand, Table 4.4 shows the peak and average loading of the BSS transformers for the single transformer mode. In this mode, all the loads are supplied by only one BSS transformer. Therefore, the BSS transformer operates near to its full capacity. The average loading of the transformer at 97.94 % lies far away from the optimum range of transformer efficiency between 40 % and 50 %.

Table 4.4 Peak and average loading of the BSS transformers in single transformer mode

Transformer (50 MVA)	Single Transformer Mode		
	Peak (MW)	Average (MW)	Average (%)
T1	58.54	48.97	97.94
T2	-	-	-

BSS transformers power loss profiles for all three operation modes are obtained from the simulations. From the power loss profiles, the 1-hour transformer losses based on the peak period are calculated and are tabulated in Table 4.5. It can be seen that the total losses of the BSS transformers in the parallel mode are lower than that of the non-parallel mode. It is also observed that the single transformer mode has the highest transformer losses.

Table 4.5 1-hour transformer losses for all three operation modes.

	Transformer Losses (kWh)		
	Non-parallel	Parallel	Single Transformer
T1	50.5	70.9	188.5
T2	101	70.9	-
Total	151.5	141.8	188.5

The percentage increment or decrement of transformer losses by parallel mode and single transformer mode compared to non-parallel mode can be calculated by using equation (15) and (16) as follows:

$$\%Losses_{diff} = \frac{Loss_{np} - Loss_p}{Loss_{np}} \times 100 \% \quad (15)$$

$$\%Losses_{diff} = \frac{Loss_{np} - Loss_s}{Loss_{np}} \times 100 \% \quad (16)$$

where $Loss_{np}$ is the 1-hour BSS transformers losses for the non-parallel mode in kWh, and $Loss_p$ is the 1-hour BSS transformers losses for the parallel mode in kWh.

As a result, we can achieve a reduction in transformer losses of 6.4 % by implementing the parallel mode for train schedules with a headway of 2 minutes. On the other hand, there will be an increase in transformer losses up to 37 % if the single transformer mode is implemented for train schedules with 2 minutes headway interval.

4.4 Impacts of Headway Variation

The results from the previous section are obtained using train schedules with 2 minutes headway. However, to cope with different passenger demands during the peak and off-peak periods, train schedules with different headway are used

from time to time. Therefore, it is necessary to investigate the transformer operations for various headways.

The main impact of increasing the headway interval is the reduction of system energy consumption. At larger headway interval, the distances between consecutive trains become larger. As a result, there is a lower total number of trains on the track at one instance. Therefore, the total system energy consumption decreases as the train headway interval increases. Figure 4.4 shows the total energy consumption of the MRT2 system in one hour, including both the varying traction loads and constant station loads at different headway.

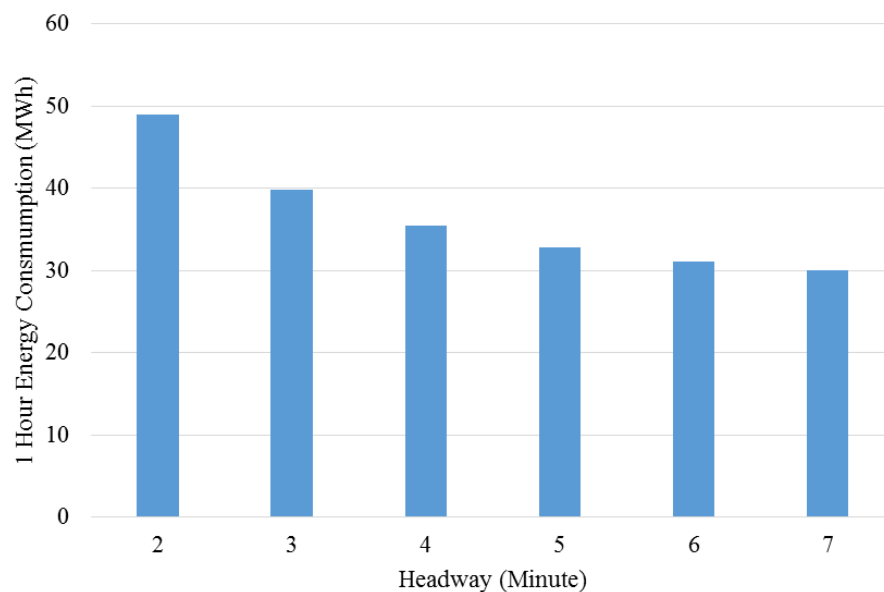


Figure 4.4 System total energy consumption at different headways

Transformer losses, which are dependent on the transformer loading, vary according to the headway. Therefore, there is a difference in transformer loss

reduction by implementing parallel mode for different headway. Table 4.6 shows the comparison of total transformer losses in one hour for non-parallel mode and parallel mode at different headway. It can be seen that the percentage of loss reduction by implementing parallel mode peaks at 3 minutes headway interval and then becomes lesser as the headway increases. This is due to the low transformer loading at larger headway interval, which leads to transformer operation shifting away from the maximum efficiency range.

Table 4.6 Total transformer losses at different headway for non-parallel mode and parallel mode

Headway (Min)	Total kWh Losses (1 hour)		Reduction of Losses by Parallel Mode (%)	Reduction of Losses by Parallel Mode (kWh)
	Non- parallel	Parallel		
2	151.5	141.83	6.39	9.67
3	122.74	114.74	6.52	8.01
4	109.9	104.05	5.32	5.85
5	103.76	98.49	5.09	5.28
6	100.15	95.03	5.11	5.12
7	97.54	92.67	4.99	4.87

On the other hand, the total transformer losses in one hour for non-parallel mode and single transformer mode at different headway are compared in Table 4.7. Results show that when the headway increases, the transformer losses in single transformer mode reduces. From the headway of 5 minutes and above, the

transformer losses for the single transformer mode becomes lower than that in non-parallel mode. In other words, the single transformer mode tends to operate at higher efficiency with train schedules of 5 minutes headway and above. This is due to the fact that in any two-transformer operation mode, the no-load losses are contributed by both the transformers. When the total energy consumption of the system decreases, the transformer no-load losses, which are independent of the transformer loading, become more significant. On the other hand, the amount of transformer no-load losses for the single transformer mode is relatively low because the no-load losses are contributed by only one transformer in operation. The results show that there is a reduction of transformer losses of up to 8.24 % for the single transformer mode for train schedules with a larger headway compared to that of non-parallel mode.

Table 4.7 Total transformer losses at different headway for non-parallel mode and single transformer mode

Headway (Min)	Total kWh Losses (1 hour)		Reduction of Losses by Single Transformer Mode (%)	Reduction of Losses by Single Transformer Mode (kWh)
	Non- parallel	Single TFS		
2	151.5	188.5	-24.42	-37
3	122.74	133.81	-9.02	-11.07
4	109.9	112.50	-2.36	-2.6
5	103.76	101.16	2.51	2.61
6	100.15	94.12	6.02	6.03
7	97.54	89.3	8.45	8.24

Table 4.8 shows the total transformer losses at different headway for parallel mode and single transformer mode. The results showed that the single transformer mode has a lower transformer loss than that of parallel mode only when the train headway interval is 6 minutes and above. This is due to the fact that the parallel mode has lower transformer losses as compared to that of the non-parallel mode. In other words, the single transformer mode is more efficient at 6 minutes headway and above as compared to both non-parallel and parallel mode.

Table 4.8 Total transformer losses at different headway for parallel mode and single transformer mode

Headway (Min)	Total kWh Losses (1 hour)		Reduction of Losses by Single Transformer Mode (%)	Reduction of Losses by Single Transformer Mode (kWh)
	Parallel	Single TFS		
2	141.83	188.5	-32.91	-46.67
3	114.74	133.81	-16.62	-19.07
4	104.05	112.50	-8.12	-8.45
5	98.49	101.16	-2.71	-2.67
6	95.03	94.12	0.96	0.91
7	92.67	89.3	3.64	3.37

Figure 4.5 shows the transformer losses for non-parallel mode, parallel mode, and single transformer mode at different headway intervals. In the figure, point X represents the intersection point between the non-parallel and single

transformer modes while point Y represents the intersection point between the parallel and single transformer modes. It can be seen that point X falls at 4 minutes 30 seconds headway interval. For any schedules with a headway interval beyond point X, it is more efficient to operate on a single transformer mode than the non-parallel mode. Point Y falls at a headway interval of 5 minutes 48 seconds. It is more efficient to implement a single transformer mode than a parallel mode for any schedules of the headway interval beyond point Y.

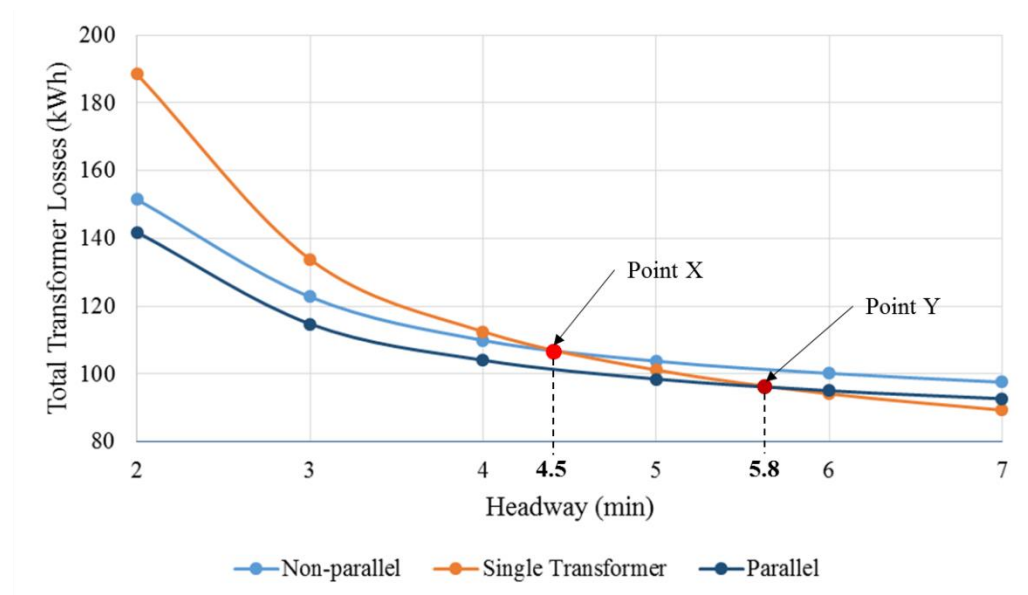


Figure 4.5 Transformer losses for different operation modes at different headway intervals

4.5 Short-circuit Analyses

From the previous section, parallel mode results in lower BSS transformer losses than the non-parallel mode. However, implementation of the parallel mode results in a higher short-circuit current. Thus, this section presents the results of

short-circuit analysis of the MRT2 traction power supply network and discusses the impact of higher short-circuit current on the system.

The short-circuit currents at the BSSs are mainly contributed by the grid. However, the auxiliary load models are assumed as the combination of motor loads and static loads. Therefore, there are short-circuit currents contributed by the auxiliary loads, particularly coming from the inertia of the rotors, which act as a power source during a fault. Although the current contribution by the auxiliary loads is very small as compared to the contribution of the grid, however it is necessary to be considered in determining the maximum short-circuit current at the faulted bus.

4.5.1 Short-circuit Current at 132 kV Level

Table 4.9 and Table 4.10 show the short-circuit current contribution from the grid and the load for non-parallel mode and parallel mode of the normal scenario for fault at 132 kV level at BSS, respectively. The maximum short-circuit current is the summation of the short-circuit current from the grid and the load at different power factors.

Table 4.9 Short-circuit current for fault at 132 kV level for non-parallel mode

Non-parallel Mode	Short-circuit Contribution (kA)		Maximum Short-circuit Current (kA)
	From Grid	From Load	
Jinjang BSS Tx1	14.5	0.136	14.63
Jinjang BSS Tx2	14.5	0.352	14.84
Kuchai Lama BSS Tx1	15	0.445	15.431
Kuchai Lama BSS Tx2	15	0.099	15.094
UPM BSS Tx1	23.7	0.09	23.786
UPM BSS Tx2	23.7	0.25	23.947

Table 4.10 Short-circuit current for fault at 132 kV level for parallel mode

Parallel Mode	Short-circuit Contribution (kA)		Maximum Short-circuit Current (kA)
	From Grid	From Load	
Jinjang BSS	14.5	0.5	14.98
Kuchai Lama BSS	15	0.572	15.551
UPM BSS	23.7	0.356	24.04

From the tables, the short-circuit currents contributed by the grid for both the operation modes are equal. However, the short-circuit contributed by the loads are slightly lower for non-parallel mode because in non-parallel mode, the loads for each BSS transformer are segregated from the other transformer. When a fault happens at the primary side of one of the BSS transformers in non-parallel mode, the loads connected to the other transformer are not affected, and thus,

not contributing any short-circuit current. On the other hand, when the fault happens at any primary side of the BSS transformers, all the loads will be affected by the fault and contribute to short-circuit current. Therefore, the total short-circuit current at 132 kV level for parallel mode is slightly higher than that in non-parallel mode, as shown in Table 4.9 and Table 4.10.

4.5.2 Short-circuit Current at 33 kV Level

Table 4.11 shows the short-circuit current when a fault happens at 33 kV Level of BSS for both non-parallel mode and parallel mode. Due to the low nominal voltage, the overall short-circuit current at 33 kV level is lower than that at 132 kV level.

Table 4.11 Short-circuit current for fault at BSSs at 33 kV level

	Maximum Short-circuit Current (kA)	
	Non-parallel	Parallel
Jinjang BSS Tx1	7.851	14.855
Jinjang BSS Tx2	8.8	14.855
Kuchai Lama BSS Tx1	9.31	15.286
Kuchai Lama BSS Tx2	7.739	15.286
UPM BSS Tx1	6.671	13.217
UPM BSS Tx2	7.401	13.217

Unlike the 132 kV level at BSSs, the short-circuit current for parallel mode is significantly higher than that for non-parallel mode at 33 kV level. This is

because in parallel mode, the buses at the primary side and the secondary side of the transformers are interconnected. The parallel connected identical transformers result in a lower equivalent impedance by half. Consequently, in this case, the short-circuit current of parallel operation is nearly double of the short-circuit current of non-parallel operation.

Figure 4.6 shows the short-circuit current for fault at all TPSSs 33 kV buses for both non-parallel mode and parallel mode of normal scenario. Similar to that at 33 kV level of the BSSs, the short-circuit current for parallel mode is much higher than the non-parallel mode, due to the lower effective impedance of the parallel connected transformers. The short-circuit current peaks at TPSS 8, TPSS 17, and TPSS 22, because they are located nearest to their respective BSS. At further the TPSS, the effective impedance from the grid to the TPSS becomes higher, resulting in a lower short-circuit current.

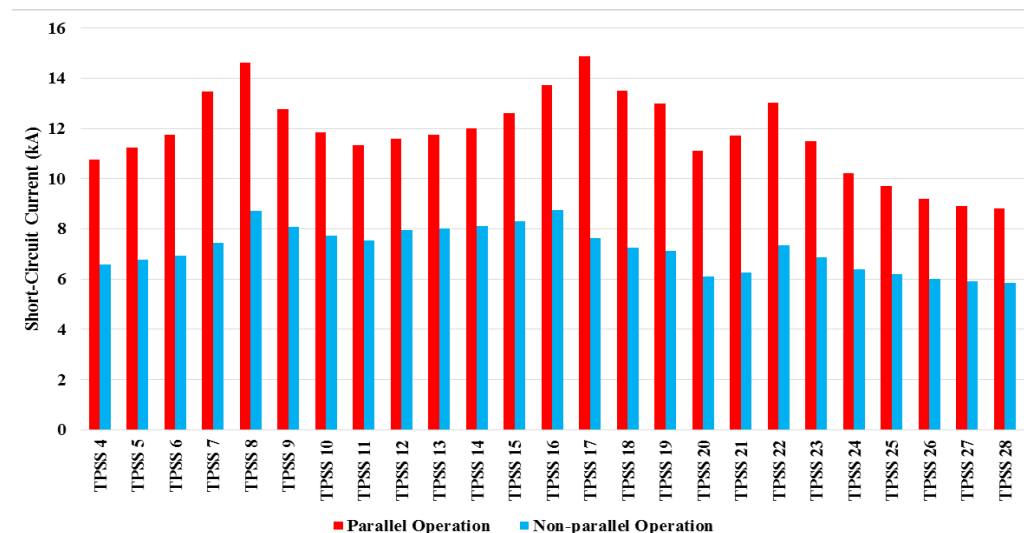


Figure 4.6 Short-circuit current for fault at all TPSSs

4.5.3 Short-circuit Current for Emergency Scenarios

Emergency scenarios happen when there is an outage of one of the BSSs, where both the BSS transformers are out of operation. The loads from the affected BSS are all supplied by the adjacent BSS, resulting in an increase of power demand at the adjacent BSS. As the adjacent BSS supplies more loads, hence there is a need to perform short-circuit analyses on the emergency scenarios.

Figure 4.7 shows the comparison of short-circuit current between emergency scenario Jinjang outage and normal scenario parallel mode. The affected TPSSs, from TPSS 4 to TPSS 11, have lower short-circuit current compared to the normal scenario parallel mode because they are further from the adjacent Kuchai Lama BSS. The short-circuit current at TPSSs on the Kuchai Lama BSS, from TPSS 12 to TPSS 19, is slightly higher than that in normal scenario parallel mode. There is no difference for short-circuit current between the emergency scenario and normal scenario parallel mode at the TPSSs on the unaffected UPM BSS, from TPSS 20 to TPSS 28. Similar explanations can be applied to the Kuchai Lama BSS outage and UPM BSS outage, as illustrated in Figure 4.8 and Figure 4.9.

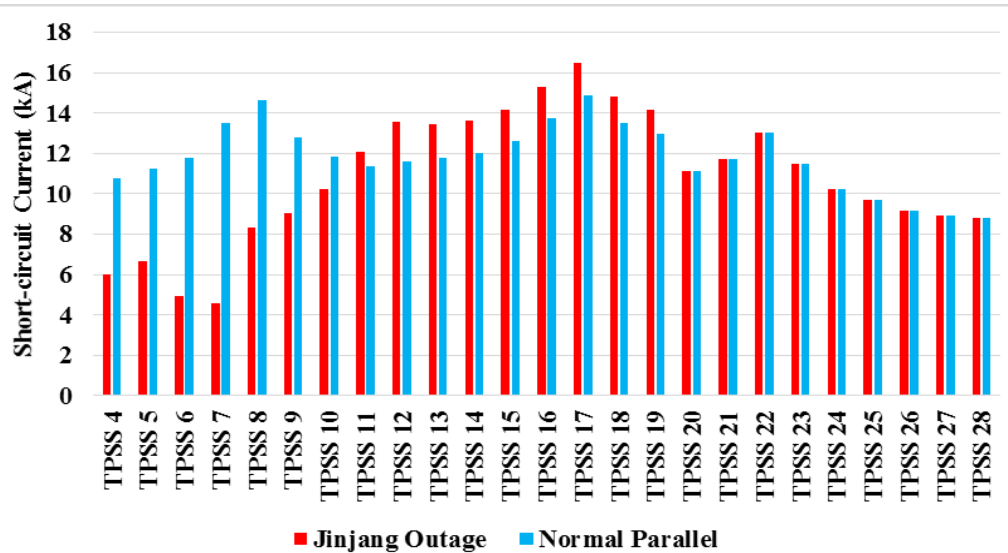


Figure 4.7 Short-circuit current of Jinjang BSS outage and normal scenario parallel mode

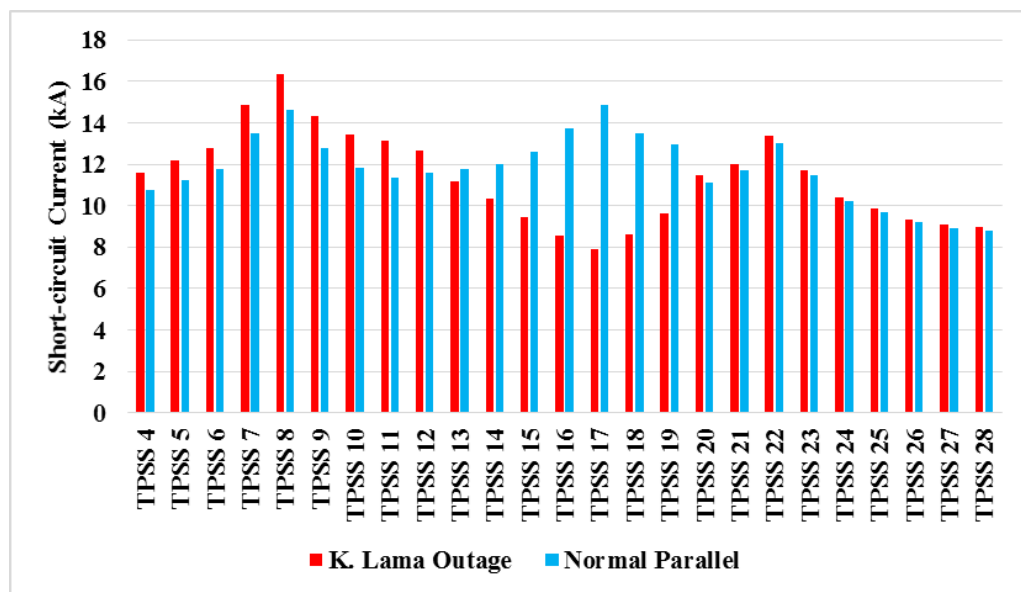


Figure 4.8 Short-circuit current of Kuchai Lama BSS outage and normal scenario parallel mode

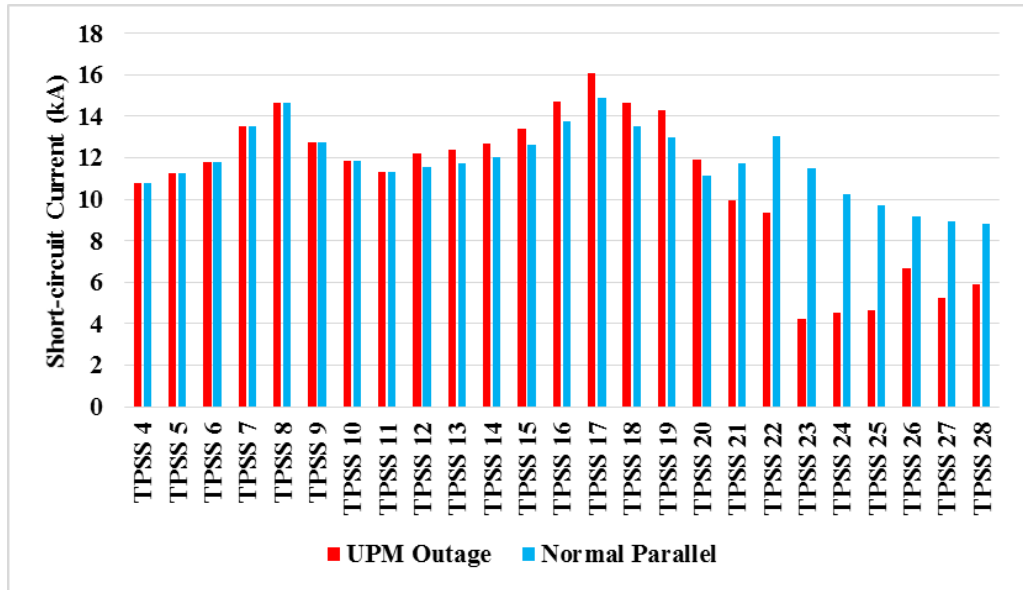


Figure 4.9 Short-circuit current of UPM BSS outage and normal scenario parallel mode

4.5.4 Impacts on Protective Devices

According to the Malaysian Distribution Code, the maximum short-circuit currents must be lower than 90 % of the short-circuit breaking withstand capability of the protective devices and the make capacity of the switchgear. However, the initial rating of the protective devices is already designed according to the worst-case scenarios, which are the emergency scenarios. Results have shown that all the maximum short-circuit currents at 132 kV level and 33 kV level at all scenarios are lower than the acceptable limits. Hence, no upgrade is needed for the protective devices to implement the parallel mode.

4.6 Investment Cost for Parallel Mode

The investment must be done to ensure a safe and robust operation of the parallel transformer operation. As mentioned earlier in Chapter 2, the challenges of implementing parallel transformer operation are the circulating current flowing in between the transformers, synchronisation of tap changers, and increases of fault level at the secondary side of the transformers. However, in this study, the flow of circulating current between the transformers is absent. The reason is that in the simulation model, both the transformers in the BSS are exactly similar with the same impedances, power ratings, voltage levels, and turn ratios.

Due to the increase of fault level by the parallel mode, the protective devices with higher kA ratings must be used in the network. However, no additional investment is needed for the protective schemes in the power supply network of the MRT2 as the protective schemes are already designed based on the worst-case emergency scenario that has a higher fault current than that of parallel mode.

An additional investment must be made to solve the synchronisation problem of tap changers between the parallel connected transformers. Unsynchronised tap changers can cause a difference in voltage level and thus results in the flow of circulating current between the transformers. The typical solution is to apply a master-follower scheme, controlled by a Remote Tap Changer Control Cubicle (RTCC) from the control room near the yard (Roy, Syamasasi and Assainar, 2015).

CHAPTER 5

CONCLUSION AND FUTURE WORKS

5.1 Conclusion

Energy efficient operation strategies for electrified railway systems have become one of the trends in the railway sector in cutting down energy costs and reducing carbon emission. The reductions of transformer losses are essentially important because transformers are one of the most important power conversion equipment. The main-tie-main configuration of BSSs in a railway system allows the BSS transformers to operate in non-parallel mode, parallel mode, or single transformer mode. The transformer losses for different operation modes are not the same for train schedules with different headway intervals. In this study, simulations have been performed to investigate the transformer losses in different operation modes with various headway intervals. A comprehensive simulation model that includes the high voltage supply network and the low voltage traction network of a railway system has been developed. Dynamic power flow analyses have been performed to accurately calculate the BSS transformer loading and loss profiles under the effect of train dynamics. To investigate the impact of parallel transformer operation on the railway system, short-circuit analyses have been performed to ensure that the maximum short-circuit currents by parallel transformer operation are within the acceptable limit.

This study is carried out based on the MRT2 power supply and distribution systems that are currently under construction. The proposed approach of loss reduction through optimal operation modes of transformers can also be applied to other DC railway systems with main-tie-main configured BSS. The percentage of transformer loss reduction, as well as the headway interval margin, may differ for different network topologies.

These are the conclusion based on the objectives defined in Chapter 1:

- 1. To develop dynamic traction load models for railway power supply network.*

A simulation model based on the MRT2 power supply and distribution system that is currently under construction has been developed. The simulation model includes the high voltage supply network and the low voltage traction network of the railway system. For the high voltage supply network, modelling of power system components including transformers, cables, and rectifiers has been done based on the parameters given by the rail operator. For the low voltage traction network modelling, the distribution network under Jinjang BSS that comprises 8 TPSSs and 15 stations, with a total track length of 17.28 km has been developed. The modelling of the rolling stocks has been done based on the data given by the rail operator and manufacturers. The tracks have been modelled according to the actual data, considering the track elevations and speed limit restrictions to simulate accurate train dynamic behaviours. The simulation model has been used to perform time-domain

power flow analyses that provide better accuracy than the conventional power adequacy study methods that consider only the worst-case scenario.

2. *To perform power adequacy studies on the railway system.*

Power adequacy studies have been done with the aid of ETAP Etrax software, to ensure the capability of the power supply network of MRT2 to supply to all the loads in all steady state conditions. With the consideration of train dynamics, load flow analyses have been performed on each time step. Thus, the simulated results incorporate the dynamic performances of all electrical components in both the high voltage supply network and the low voltage traction network. Results have shown that the power supply network is capable to cover all loads in all scenarios. The average BSS transformer loadings for all the operation modes are calculated, and the results showed that the BSS transformers operate nearest to the transformer maximum efficiency point in parallel mode.

3. *To evaluate the optimal operation mode of the transformers with different train schedules with the final aim of achieving power loss reduction.*

The power loss profiles of the BSS transformers for all operation modes have been obtained from the power adequacy studies. The 1-hour transformer losses at the peak period have been extracted from the power loss profiles. By comparing the total transformer losses in all three operation modes, the optimal operation mode of the transformers which has the highest energy efficiency and lowest power losses has been found.

This study has proven that the parallel mode has as much as 6.52 % lower losses than that of the non-parallel mode for all the headway intervals. The optimal operation mode of BSS transformers at different headway interval has been found. Results have also shown that the single transformer mode is the most energy efficient mode when the headway interval increases above 5 minutes 48 seconds, while parallel mode has the lowest transformer losses when the headway interval is below 5 minutes 48 seconds.

4. *To observe the impact of parallel transformer operation on the short-circuit current of a railway system.*

Short-circuit analyses in accordance with standard IEC 60909 have been performed on non-parallel mode and parallel mode to observe the increment of maximum short-circuit current by the parallel transformer operation. Results have shown that by implementing parallel mode, there is a negligible increment of maximum short-circuit current at 132 kV level of BSSs, but the maximum short-circuit current is significantly higher at 33 kV level of BSSs and TPSSs. Results have further shown that in emergency scenarios, the maximum short-circuit current at 33 kV level of TPSSs under the adjacent BSS of the faulted bus is slightly higher than that in normal scenario parallel mode. However, all the maximum short-circuit currents at 132 kV level and 33 kV level at all scenarios are within the acceptable limits with present switchgear and protective device ratings. Hence, no upgrade is needed for the protective devices to implement the parallel mode.

5.2 Limitations and future works

There are several limitations to this research work. Firstly, regenerative braking is not considered in this study. An accurate simulation of regenerative braking requires a robust operating strategy for the coordination of rectifiers and inverters in the TPSSs, which is out of the scope of this research. Incorporating the recovered energy from the braking of vehicles would reduce the total power demand and net energy consumption of the railway system. In fact, the impact of regenerative braking could be significant for a system with optimised strategies to increase the utilisation of regenerative energy. However, the simulations in this study are based on the basic operating strategies without consideration of maximising the utilisation of regenerative energy. Without timetable optimisation and installation of ESSs in the simulation, the recovered energy was dissipated through the dedicated resistor banks, and this process is isolated from the railway power traction network. Thus, the impact of regenerative braking on the simulations in this study is not significant.

Secondly, a simple timetable model is used in this study. The timetable has a constant station dwell time of 30 seconds, which is not realistic in a railway system. In the actual case, in order to cope with the higher passenger flow in certain locations, the train dwell time for the stations in the busy areas would be set to a longer period. In addition, there will be a dwell time 'noise' due to stochastic interruptions, which cause the unequal dwell time whenever a train

stops at the stations. These factors could cause variations in the BSS transformer loadings, which in turn, would change the value of total transformer losses.

Thirdly, the same power profile is used for all the trains in each station. In other words, the total weight of the trains is assumed to be constant throughout the journey. In reality, however, the weight of a vehicle keeps changing after stopping at each station, depending on the net influx of the passenger into the vehicle. A change in total train weight would cause different results on the train rolling resistance, gradient resistance, the required tractive effort during the acceleration phase, and total energy consumption of the train.

The future work should include the regenerative braking into the simulations to obtain a more realistic result. To achieve this, a control strategy for the operation and coordination of the inverters and rectifiers should be developed. An optimised timetable model that maximises the utilisation of regenerative braking while considering the dwell time ‘noise’ should be developed. A more comprehensive transformer model should be developed and integrated into the ETAP model to accurately validate the relationship between transformer loading and transformer efficiency. With a more realistic simulation, the loss reduction rate of the proposed approach can be rigidly justified.

LIST OF REFERENCES

- Alfieri, L., Battistelli, L. and Pagano, M. (2019) 'Impact on railway infrastructure of wayside energy storage systems for regenerative braking management: A case study on a real Italian railway infrastructure', *IET Electrical Systems in Transportation*, 9(3), pp. 140–149. doi: 10.1049/iet-est.2019.0005.
- Almaksour, K. *et al.* (2020) 'Comparison of dynamic models for a DC railway electrical network including an AC/DC bi-directional power station', *Mathematics and Computers in Simulation*, (xxxx). doi: 10.1016/j.matcom.2020.05.027.
- Arboleya, P. and Armendariz, U. (2016) 'Energy is on board: energy storage and other alternatives in modern light railways', *IEEE Electrification Magazine*, 4(SEPTEMBER), pp. 30–41. doi: 10.1109/MELE.2016.2584938.
- Borge-Diez, D. *et al.* (2013) 'Parallel distribution transformer loss reductions: A proposed method and experimental validation', *International Journal of Electrical Power and Energy Systems*, 49(1), pp. 170–180. doi: 10.1016/j.ijepes.2012.12.006.
- Brosan, G. S. and Bishop, D. O. (1960) 'An optimum ratio of copper losses and iron losses for a transformer with variable load', *Proceedings of the IEE Part C: Monographs*, 107(11), p. 98. doi: 10.1049/pi-c.1960.0013.
- Cantor, E. L. *et al.* (2012) 'Allocation of active power filter in DC traction systems', *European Transactions on Electrical Power*. doi: 10.1002/etep.
- Ceraolo, M. *et al.* (2018) 'Energy storage systems to exploit regenerative braking in DC railway systems: Different approaches to improve efficiency of modern high-speed trains', *Journal of Energy Storage*, 16, pp. 269–279. doi: 10.1016/j.est.2018.01.017.
- Chen, L. *et al.* (2016) 'Ancillary Service for Transmission Systems by Tap Stagger Operation in Distribution Networks', *IEEE Transactions on Power Delivery*, 31(4), pp. 1701–1709. doi: 10.1109/TPWRD.2015.2504599.
- Chuang, H. *et al.* (2008) 'Design of Optimal Coasting Speed for Saving Social Cost in Mass Rapid Transit Systems', in *2008 Third International Conference on Electric Utility Deregulation and Restructuring and Power Technologies*, pp. 2833–2839.
- Chymera, M. and Goodman, C. J. (2006) 'Overview of Electric Railway Systems and the Calculation of Train Performance', in *The 9th Institution of Engineering and Technology Professional Development Course on Electric Traction Systems*, pp. 1–18.
- Colas Rail System Engineering Sdn. Bhd. (2018a) *Mainline Traction Modelling Report*.
- Colas Rail System Engineering Sdn. Bhd. (2018b) *MRT2 SSP HV Modelling*

Report.

Cornic, D. (2010) 'Efficient recovery of braking energy through a reversible dc substation', in *International Conference on Electrical Systems for Aircraft, Railway and Ship Propulsion, ESARS 2010*. IEEE. doi: 10.1109/ESARS.2010.5665264.

Domínguez, M. *et al.* (2014) 'Multi objective particle swarm optimization algorithm for the design of efficient ATO speed profiles in metro lines', *Engineering Applications of Artificial Intelligence*, 29, pp. 43–53. doi: 10.1016/j.engappai.2013.12.015.

Fabre, J., Ladoux, P. and Piton, M. (2015) 'Characterization and Implementation of Dual-SiC MOSFET Modules for Future Use in Traction Converters', *IEEE Transactions on Power Electronics*, 30(8), pp. 4079–4090.

Fernández-rodríguez, A. *et al.* (2015) 'Design of Robust and Energy-Efficient ATO Speed Profiles of Metropolitan Lines Considering Train Load Variations and Delays', *IEEE Transactions on Intelligent Transportation Systems*, 16(4), pp. 2061–2071. doi: 10.1109/TITS.2015.2391831.

García-olivares, A., Solé, J. and Osychenko, O. (2018) 'Transportation in a 100 % renewable energy system', *Energy Conversion and Management*, 158(August 2017), pp. 266–285. doi: 10.1016/j.enconman.2017.12.053.

Gelman, V. (2013) 'Energy Storage That May Be Too Good to Be True', *IEEE Vehicular Technology Magazine*, pp. 70–80.

Ghaviha, N. *et al.* (2017) 'Review of Application of Energy Storage Devices in Railway Transportation', *Energy Procedia*, 105, pp. 4561–4568. doi: 10.1016/j.egypro.2017.03.980.

González-Gil, A., Palacin, R. and Batty, P. (2013) 'Sustainable urban rail systems: Strategies and technologies for optimal management of regenerative braking energy', *Energy Conversion and Management*, 75, pp. 374–388. doi: 10.1016/j.enconman.2013.06.039.

Harden, K. D. (2011) *Optimizing Energy Efficiency Standards for Low Voltage Distribution Transformers*. Purdue University. Available at: <https://www.pfw.edu/dotAsset/bea78c04-bbef-424f-9397-45bac5641842.pdf> (Accessed: 14 February 2019).

Huang, Y. *et al.* (2014) 'Distribution network load distribution strategy considering the economy of parallel transformers', in *33rd Electrical Insulation Conference, EIC 2015*. IEEE, pp. 114–117. doi: 10.1109/ICACACT.2014.7223480.

'IEC 60909–0:2016: Short-circuit currents in three-phase a.c. systems - part 0: Calculation of currents' (2016) *International Standard*.

IEEE Standards Association (2015) 'IEEE Guide for Paralleling Regulating Transformers IEEE Power and Energy Society', *IEEE Std C57.153TM-2015*. doi: 10.1109/IEEESTD.2015.7118615.

International Energy Agency (2020a) *Rail*. Available at: <https://www.iea.org/reports/rail>.

- International Energy Agency (2020b) *The Future of Rail*. Available at: <https://www.iea.org/reports/the-future-of-rail>.
- Jakus, D. and Vasilj, J. (2018) ‘Optimising the transformer substation topology in order to minimise annual energy losses’, *IET Generation, Transmission & Distribution*, 12(1), pp. 1323–1330. doi: 10.1049/iet-gtd.2017.0721.
- Jaramillo-Duque, Á. *et al.* (2018) ‘Power loss minimization for transformers connected in parallel with taps based on power chargeability balance’, *Energies*, 11(2). doi: 10.3390/en11020439.
- Jauch, E. T. (2006) ‘Factors in choosing transformer paralleling methods’, *Proceedings of the IEEE Power Engineering Society Transmission and Distribution Conference*, pp. 1064–1069. doi: 10.1109/TDC.2006.1668649.
- Jean-Paul Rodrigue (2020) *The Geography of Transport Systems*. 5th edn. New York: Routledge.
- Kampeerawat, W. and Koseki, T. (2017) ‘A strategy for utilization of regenerative energy in urban railway system by application of smart train scheduling and wayside energy storage system’, *Energy Procedia*, 138, pp. 795–800. doi: 10.1016/j.egypro.2017.10.070.
- Knesebeck, J. von dem (2011) *Transit Systems of the US and Germany - A Comparison*. Georgia Institute of Technology.
- Konishi, T. and Tobita, M. (2012) ‘Fixed energy storage technology applied for DC electrified railway (traction power substation)’, in *Electrical Systems for Aircraft, Railway and Ship Propulsion, ESARS*. IEEE. doi: 10.1109/ESARS.2012.6387438.
- Kumar, N. *et al.* (2012) *Power Plant Cycling Costs*. National Renewable Energy Laboratory.
- Lee, H. *et al.* (2013) ‘Peak power reduction and energy efficiency improvement with the superconducting flywheel energy storage in electric railway system’, *Physica C: Superconductivity and its Applications*, 494, pp. 246–249. doi: 10.1016/j.physc.2013.04.033.
- Lin, S., Song, W. and Feng, Z. (2014) ‘Simulation research on rail transit traction grid voltage stabilization and its energy saving effects based on BESS’, *International Journal of Smart Grid and Clean Energy*, 3(4), pp. 431–436. doi: 10.12720/sgce.3.4.431-436.
- Liu, H. *et al.* (2019) ‘Timetable Optimization for Regenerative Energy Utilization in Subway Systems’, *IEEE Transactions on Intelligent Transportation Systems*, 20(9), pp. 3247–3257. doi: 10.1109/TITS.2018.2873145.
- Lu, S. *et al.* (2013) ‘Single-Train Trajectory Optimization’, *IEEE Transactions on Intelligent Transportation Systems*, 14(2), pp. 743–750. doi: 10.1109/TITS.2012.2234118.
- Malaysian Energy Commission (2017) ‘Distribution code for Peninsular Malaysia, Sabah & F.T. Labuan’. Available at: http://www.dcode.org.uk/assets/uploads/DCode_Summary-May_2017.pdf.

- Meishner, F. and Sauer, D. U. (2019) 'Wayside energy recovery systems in DC urban railway grids', *eTransportation*, 1, p. 100001. doi: 10.1016/j.etrans.2019.04.001.
- Ogasa, M. and Taguchi, Y. (2007) 'Power flow control for hybrid electric vehicles using trolley power and on-board batteries', *Quarterly Report of RTRI (Railway Technical Research Institute) (Japan)*, 48(1), pp. 30–36. doi: 10.2219/rtriqr.48.30.
- Okui, A. *et al.* (2010) 'Application of energy storage system for railway transportation in Japan', in *2010 International Power Electronics Conference - ECCE Asia -, IPEC 2010*. IEEE, pp. 3117–3123. doi: 10.1109/IPEC.2010.5542321.
- Palacin, R., Batty, P. and Powell, J. P. (2014) 'A systems approach to reduce urban rail energy consumption', *Energy Conversion and Management*, 80, pp. 509–524. doi: 10.1016/j.enconman.2014.01.060.
- Qu, Y. *et al.* (2020) 'Robust optimization of train timetable and energy efficiency in urban rail transit: A two-stage approach', *Computers and Industrial Engineering*, 146(May), p. 106594. doi: 10.1016/j.cie.2020.106594.
- Ratniyomchai, T., Hillmanssen, S. and Tricoli, P. (2014) 'Optimal capacity and positioning of stationary supercapacitors for light rail vehicle systems', in *2014 International Symposium on Power Electronics, Electrical Drives, Automation and Motion, SPEEDAM 2014*. IEEE, pp. 807–812. doi: 10.1109/SPEEDAM.2014.6872019.
- Roch-dupré, D. *et al.* (2021) 'Determining the optimum installation of energy storage systems in railway electrical infrastructures by means of swarm and evolutionary optimization algorithms', *Electrical Power and Energy Systems*, 124(January 2020), p. 106295. doi: 10.1016/j.ijepes.2020.106295.
- Roy, R., Syamasasi, J. and Assainar, J. (2015) 'Tap Changing in Parallel Operated Transformers Using SCADA', *International Journal of Advanced Research in Electrical, Electronics and Instrumentation Engineering*, 4(4), pp. 1871–1875.
- Serrano-Jiménez, D. *et al.* (2017) 'Electrical railway power supply systems: Current situation and future trends', *International Journal of Electrical Power and Energy Systems*, 92, pp. 181–192. doi: 10.1016/j.ijepes.2017.05.008.
- Srivastava, J., Kumar Singh, V. and Singhal, A. (2013) 'Review on Railway Traction Power Supply System', *Journal of Environmental Science , Computer Science and Engineering & Technology*, 2(4), pp. 1236–1250.
- Steiner, M., Klohr, M. and Pagiela, S. (2007) 'Energy storage system with Ultracaps on board of railway vehicles', in *2007 European Conference on Power Electronics and Applications, EPE*. doi: 10.1109/EPE.2007.4417400.
- Su, S. *et al.* (2014) 'Energy-efficient train control in urban rail transit systems', *Journal of Rail and Rapid Transit*. doi: 10.1177/0954409713515648.
- Su, S., Tang, T. and Wang, Y. (2016) 'Evaluation of Strategies to Reducing Traction Energy Consumption of Metro Systems Using an Optimal Train

Control Simulation Model’, pp. 1–19. doi: 10.3390/en9020105.

Takagi, R. and Amano, T. (2015) ‘Optimisation of reference state-of-charge curves for the feed-forward charge/discharge control of energy storage systems on-board DC electric railway vehicles’, *IET Electrical Systems in Transportation*, 5(1), pp. 33–42. doi: 10.1049/iet-est.2012.0014.

Teymourfar, R. *et al.* (2012) ‘Stationary super-capacitor energy storage system to save regenerative braking energy in a metro line’, *Energy Conversion and Management*, 56, pp. 206–214. doi: 10.1016/j.enconman.2011.11.019.

Tian, Z. (2017) *System Energy Optimisation Strategies for DC Railway Traction Power Networks*. University of Birmingham.

Tomita, M. *et al.* (2010) ‘Development of prototype DC superconducting cable for railway system’, *Physica C: Superconductivity and its applications*, 470, pp. S1007–S1008. doi: 10.1016/j.physc.2010.03.014.

Verdicchio, A. *et al.* (2019) ‘Future DC Railway Electrification System - Go for 9 kV’, in *2018 IEEE International Conference on Electrical Systems for Aircraft, Railway, Ship Propulsion and Road Vehicles and International Transportation Electrification Conference, ESARS-ITEC 2018*. IEEE. doi: 10.1109/ESARS-ITEC.2018.8607304.

White, R. D. D. (2015) ‘AC / DC Railway Electrification and Protection’, (December). doi: 10.1049/cp.2014.1439.

Wu, C. *et al.* (2020) ‘Optimal Sizing of Onboard Energy Storage Devices for Electrified Railway Systems’, *IEEE Transactions on Transportation Electrification*, 6(3), pp. 1301–1311. doi: 10.1109/TTE.2020.2996362.

Yang, X. *et al.* (2014) ‘A two-objective timetable optimization model in subway systems’, *IEEE Transactions on Intelligent Transportation Systems*, 15(5), pp. 1913–1921. doi: 10.1109/TITS.2014.2303146.

Yang, X. *et al.* (2016) ‘A Survey on Energy-Efficient Train Operation for Urban Rail Transit’, *IEEE Transactions on Intelligent Transportation Systems*, 17(1), pp. 2–13. doi: 10.1109/TITS.2015.2447507.

Zaboli, A. *et al.* (2017) ‘Evaluation and Control of Stray Current in DC-Electrified Railway Systems’, *IEEE Transactions on Vehicular Technology*, 66(2), pp. 974–980. doi: 10.1109/TVT.2016.2555485.